Control Engineering Practice 62 (2017) 55–69

Contents lists available at ScienceDirect

Control Engineering Practice

journal homepage: www.elsevier.com/locate/conengprac

Issues in closed-loop needle steering☆

Carlos Rossa, Mahdi Tavakoli

Department of Electrical and Computer Engineering, University of Alberta, Edmonton, Canada

ARTICLE INFO

Keywords:
Feedback control
Surgical robotics
Robotic assistance
Steerable needles
Sensors

ABSTRACT

Percutaneous needle insertion is amongst the most prevalent clinical procedures. The effectiveness of needle-base interventions heavily relies on needle targeting accuracy. However, the needle interacts with the surrounding tissue during insertion and deflects away from its intended trajectory. To overcome this problem, a significant research effort has been made towards developing robotic systems to automatically steer bevel-tipped needles percutaneously, which is a comprehensive and challenging control problem. A flexible needle inserted in soft tissue is an under-actuated system with nonholonomic constraints. Closed-loop feedback control of needle in tissue is challenging due to measurement errors, unmodelled dynamics created by tissue heterogeneity, and motion of targets within the tissue. In this paper, we review recent progress made in each of the complementary components that constitute a closed-loop needle steering system, including modelling needle-tissue interaction, sensing needle deflection, controlling needle trajectory, and hardware implementation.

1. Introduction

Surgical robotics has significantly grown over the past decade to enable the use of robotic systems in various complex medical procedures that are arguably impossible to perform with conventional means. Robotic systems are used to augment and extend the capabilities of surgeons, offering great levels of dexterity and precision in diagnosis and treatment. The goal of surgical robotics is not to replace the surgeon, but rather to extend his/her capabilities. Thus, one often refers to surgical robots as assistants that work in tandem with surgeons (Taylor et al., 2008).

A special subclass of these systems is devoted to minimally invasive surgery and therapy (MIST), where the surgeon inserts the surgical tools into the patient's body through small incisions or natural orifices. To date, MIST has been deployed in numerous clinical scenarios including treatments for cancers (Advincula and Song, 2007; Giulianotti et al., 2010; Kang et al.,2009; Kim et al., 2010; Luketich et al., 2003), radio-frequency and microwave ablation of liver and lung (Boctor et al., 2004), treatments for astroesophageal reflux disease (Chapman et al.,2001), gastric bypass and banding (Nguyen et al.,2001), uterine fibroids and prolapse (Falcone and Bedaiwy, 2002), benign cervical disorders (Tinelli et al., 2011), mitral valve prolapse and repair (Nifong et al., 2003), atrial septal defect (Morgan et al.,2004), atrial fibrillation (Di Biase et al., 2009), kidney disorders (Horgan et al., 2002), and bariatric (Gill et al.,2011) and prostate surgeries (Lanfranco et al., 2004). When compared to open surgery, MIST has been shown to reduce pain and blood loss, lower risk of infections, shorten hospital stay, and quicken recovery time.

Irrespective of the application, precise system performance and patient safety are shared requirements in these systems. Examples of the former include accurate steering of flexible needles during percutaneous soft-tissue insertions subject to tissue inhomogeneity and limited control over the needle trajectory, surgical instrument control under physiological organ motion in surgery on a beating heart (Bowthorpe & Tavakoli, 2016), image-guided control and motion tracking of medical instruments (Glozman & Shoham, 2007; West & Maurer, 2004), and optimal trajectory planning for deformable catheters (Gayle et al., 2005). Regarding patient safety, surgical robots can show a large variety of extent of automation. Some are held and operated directly by the surgeon and supplement the ability of the surgeon to perform operations inside the patient's body with superhuman dexterity and precision. Others rather work in tandem with the surgeon and perform functions such as orienting and stabilizing an ultrasound probe or keeping a surgical tool still.

One may surmise that the higher the autonomy granted to the surgical robot, the higher the risk of injuring the patient if the system performance is mediocre or if it becomes unstable (Fei et al.et al., 2001). A medical tool operating under feedback control is vulnerable to various sources of disturbances. Amongst other factors, a surgical instrument that interacts with deformable tissue is subject to uncer-

☆ This work was supported by the Natural Sciences and Engineering Research Council (NSERC) of Canada [grant CHRP 446520], the Canadian Institutes of Health Research (CIHR) [grant CPG 127768], and by the Alberta Innovates - Health Solutions (AIHS) [grant CRIO 201201232].

E-mail addresses: rossa@ualberta.ca (C. Rossa), mahdi.tavakoli@ualberta.ca (M. Tavakoli).

http://dx.doi.org/10.1016/j.conengprac.2017.03.004
Received 16 January 2017; Received in revised form 8 March 2017; Accepted 11 March 2017

tainties arising from the contact with the tissue (Abolhassani et al. 2007), measurement noise and delay (Bowthorpe et al., 2014) including image registration errors (Grimson et al., 1996), and poor visualization of the task being performed (Keereweer et al., 2011). Treating these systems from a closed-loop feedback control perspective will allow us to highlight the trade-off that exists between system performance, patient safety, and clinical translation of robotic technologies.

To illustrate the above problem, in this paper we will focus on control issues in percutaneous needle steering; a particularly challenging subclass of MIST. Percutaneous needle insertion has become part of routine clinical practice for tissue sampling, pinpoint drug delivery, permanent brachytherapy, radiofrequency and microwave ablation of liver, lung, and kidney, and regional anaesthesia. The success of these procedures heavily relies on accurate needle placement within an inner body target location. Bevel-tipped needle steering is particularly challenging. Firstly, a flexible needle inserted in soft tissue is an under-actuated system whose equilibrium condition is never reached as it travels in tissue. Secondly, the needle and tissue form a high-dimensional coupled system subject to uncertainties and disturbances arising from tissue heterogeneity and deformation, anisotropy, anatomic organ motion, and target displacement. These observations make the needle steering in soft tissue a challenging control problem.

This paper is not intended to be a traditional survey on surgical robotics. Rather, we will narrow our focus to the different subsystems that are needed for closed-loop feedback control of flexible needles in percutaneous therapy. This survey is based on the author's extensive work on modelling (Carriere et al., 2015; Fallahi et al., 2015a, 2015b, 2016a, 2016b; Rossa & Tavakoli, 2016; Rossa et al., 2016; Rossa et al., 2016b; Waine et al., 2016), sensing (Carriere et al. 2016; Fallahi et al. 2016; Lehmann et al., 2015, 2016; Waine et al., 2016; Waine, 2016), control (Fallahi et al., 2016; Khadem et al., 2016a, 2016b; Lehmann et al., 2016; Rossa et al., 2016; Waine et al., 2016), and design (Khadem et al., 2016a; Rossa et al., 2016b; Rossa, Usmani, Sloboda, & Tavakoli, 2017) of robotics-assisted needle steering. As a starting point for our discussion, let us consider the fully automated needle steering system depicted in Fig. 1. The issues addressed in this paper arise from each of the subsystems that compose the fully automated closed-loop system i.e., (1) Modelling needle-tissue interaction for trajectory prediction, (2) Sensing needle tip deflection; (3) Model-based and non-model-based controller design; and (4) Collaborative vs. fully automated steering.

The rest of the paper is organized around each of the above points, which will be discussed in details from Sections 2–5, respectively. A discussion on open challenges regarding each of these points will then conclude the paper.

2. Needle-tissue interaction modelling

Here we will consider steerable needles with an asymmetric beveled tip inserted in soft tissue. The needle's mechanical behaviour during insertion depends on the coupled deformations of both the needle shaft and the surrounding tissue. The interaction can be classified into four distinct phases as illustrated in Fig. 2, i.e., tissue puncturing, tissue cutting, needle-tissue friction, and tissue deformation (Misra et al. et al., 2008; Okamura et al., 2004).

Tissue puncturing: Puncturing happens at the initial contact between the needle tip and the tissue. It starts by deforming the tissue and continues until the contact force reaches its maximum and a crack is formed in the tissue surface. Puncturing results in a relatively large force at the needle tip that drops when the needle tip enters the tissue (Khadem et al., 2016; Misra et el., 2008; Okamura et al., 2004).

Tissue cutting: As the needle tip further advances into tissue, it displaces the immediate surrounding tissue and the crack grows, creating the effect of tissue cutting (Khadem et al., 2016b). Considering the tissue as an elastic medium, tissue compression at the needle tip leads to a distributed load being applied on both sides of the needle tip that, due to the asymmetric bevel tip, results a net force normal to the needle shaft (Q in Fig. 2) (Misra et al., 2010).

Friction: Friction is applied tangentially to the needle shaft against the motion of the needle (see Fig. 2). Three regimes of interest exist: (1) The static friction while the needle is in steady state, (2) the transition from the steady state to the sliding state, and (3) the velocity-dependent forces as the needle moves (Asadian et al., 2011; Khadem et al., 2016). Friction contributes to tissue displacement along the needle shaft but does not have a significant effect on needle deflection (Misra et al., 2010).

Tissue deformation: The force Q applied at the needle tip makes the needle bend and follow a curved trajectory as it moves. Consequently, the deformed needle shaft compresses the surrounding tissue, which in turn applies forces to the needle shaft and influences the tip trajectory (Khadem et al., 2016a). Tissue reaction forces are applied perpendicularly to the contact surface between the needle shaft and the tissue. Therefore, needle deflection and tissue deformation are coupled effects that influence each other (Rossa et al. 2016a; Wan et al., 2005).

From a control perspective, the bevelled tip has antagonistic effects: As it facilitates cutting and penetrating the tissue, it also increases the deflection as the needle advances. Thus, twisting the needle base axially

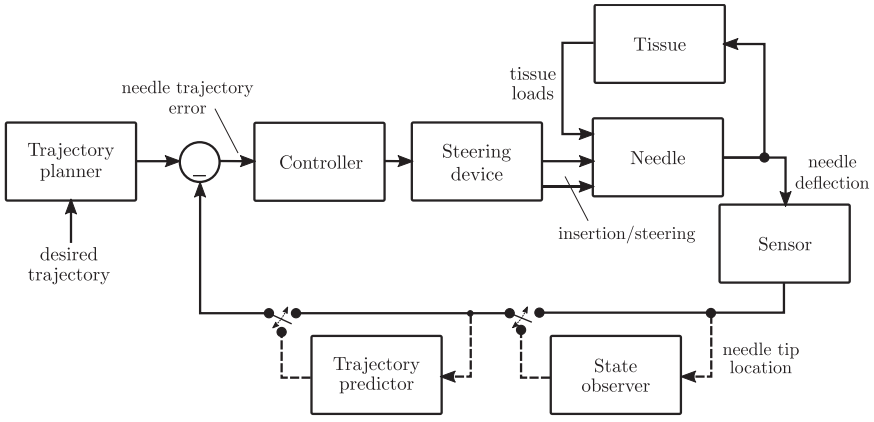

Fig. 1. Block diagram of feedback control for fully-automated needle steering illustrates the concept of using a measurement of needle tip position to control the system by comparing its output to a desired trajectory.

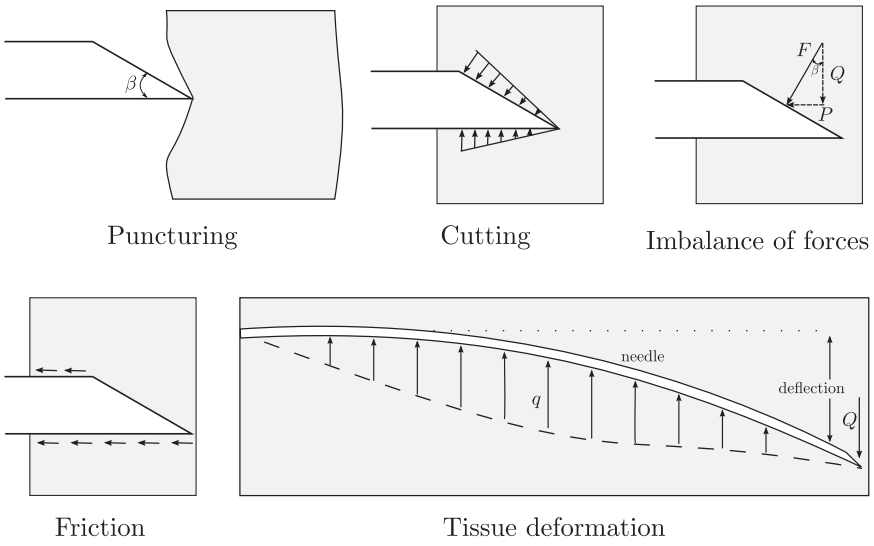

Fig. 2. Needle-tissue interaction during insertion. As a bevelled-tip needle advances in soft tissue, the needle tip cuts and displaces the tissue and a force F is created normal to the bevel. The resultant vertical force $Q = F\cos(\phi)$, where ϕ is the bevel angle, causes the needle to bend and deform the surrounding tissue, resulting in the distributed load q being applied to the needle shaft.

changes the direction of the tip force Q and provides steering capabilities. A proper combination of insertion depth and rotation can then be used in order to control the trajectory of the needle tip. A needle with symmetric tip would not provide enough control inputs to compensate for deflection that would arise from interactions with non-homogeneous tissue anyway.

Similar to a bicycle or a car, the forward motion of the needle in tissue is subject to nonholonomic constraints, i.e., the needle cannot instantaneously move in arbitrary directions. The needle is an under-actuated system that is not locally controllable, i.e., any state close to the current state is not reachable in arbitrarily small amounts of time by paths close to the current state (Haddadi et al., 2010). The needle can be manoeuvred within tissue by reorienting the bevel-tip through twists applied to the needle base. The flexible needle shaft bends due to reaction forces from the tissue, causing the needle to follow paths with variable curvatures (Kataoka et al., 2001). To control the states of a flexible needle, mainly only three inputs are available, i.e., needle insertion, needle base twists, and needle base lateral motion. The next subsection review some of the most common models used to represent needle-tissue interactions.

2.1. Nonholonomic kinematics

The simplest and perhaps the most widespread model of needle-tissue interaction is the nonholonomic model first introduced in Webster et al. (2006) and derived in its current form in Cowan et al. (2011). Essentially, it describes the forward motion of bevelled-tip needles in tissue as a bicycle with a fixed front wheel angle. A simplified 2-dimensional (2D) version is shown in Fig. 3a. The model is composed of two hypothetical wheels placed at a distance a and b from the needle tip, and oriented by an angle ϕ with respect to each other. The steering angle makes it follow a circular path whose radius of curvature κ is empirically determined for a given needle and tissue. This arrangement constrains the needle motion to follow a path with a constant curvature, which can be reversed by rotating the needle base axially by 180°.

Fig. 3b shows a representation of the needle in 3D space. The position and orientation of the needle tip coincide with that of the moving frame $\{B\}$ attached to the needle tip, with respect to the fixed inertial frame $\{A\}$. In generalized coordinates defined as $p = [x(t), y(t), z(t), \alpha(t), \beta(t), \gamma(t)]$, the nonholonomic model is given by

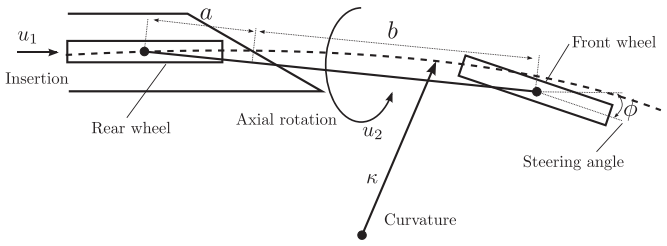

(a) Nonholonomic needle model

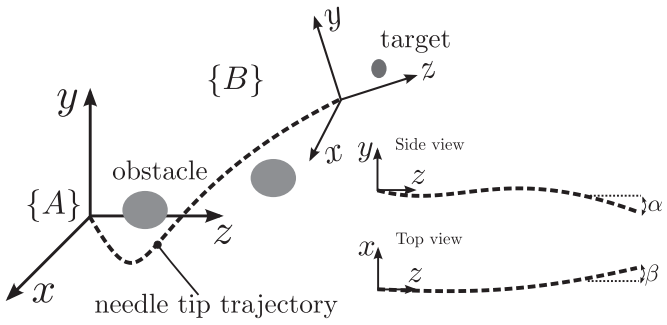

(b) Needle trajectory in 3D space

Fig. 3. Nonholonomic model of needle steering in non-deformable tissue. (a) shows the bicycle model of the needle composed of two wheels oriented by an angle ϕ with respect to each other. In (b), the resulting needle tip trajectory. Frame $\{A\}$ is fixed and the moving frame $\{B\}$ is attached to the needle tip.

$$\begin{bmatrix}\dot{x}\\ \dot{y}\\ \dot{z}\\ \dot{\alpha}\\ \dot{\beta}\\ \dot{\gamma}\end{bmatrix} = \begin{bmatrix}\sin(\beta) & 0\\ -\cos(\beta)\sin(\alpha) & 0\\ \cos(\alpha)\cos(\beta) & 0\\ \kappa\cos(\gamma)\sec(\beta) & 0\\ \kappa\sin(\gamma) & 0\\ -\kappa\cos(\gamma)\tan(\beta) & 1\end{bmatrix} \times \begin{bmatrix}u_1\\ u_2\end{bmatrix}, \tag{1}$$

where x, y, and z refer to the position of the needle tip, while α, β, and γ are the yaw, pitch and roll of the needle tip, respectively. The system is driven with two control inputs, namely the insertion velocity u_1 and the axial rotation velocity of the needle base u_2 written in frame $\{A\}$. The

dot operator $\dot{\{\}}$ represents the first derivative with respect to time t.

For simplicity, the needle tip trajectory is assumed to be the same as the needle shaft, which implies that the tissue is stiff relative to the needle. In practice, however, this assumption does not hold since the needle deflects and compresses the surrounding tissue, which in turn applies forces to the needle affecting its trajectory. To account for tissue displacement, a recent extension to this model has been proposed in Fallahi et al. (2015). The back wheel is replaced with an omnidirectional wheel that can move sideways, allowing the needle to follow a path with a variable radius of curvature thanks to the additional degree of freedom added by the slippage of the back wheel. As in Webster et al. (2006), the model must be calibrated to a given needle and tissue, and for a given insertion velocity. It has been demonstrated that the model accuracy decreases with the insertion velocity due to the increasing tissue cutting force (Khadem et al., 2016b).

The principal limitation of the model in (1) is the fact that only the position of the needle tip is estimated and all forces applied by the tissue along the needle shaft cannot be calculated. Yet, this information is critical in order to account for target displacement and other loads applied to the needle during insertion. To address this, finite elements modelling has been proposed.

2.2. Finite Elements Models

Finite Elements Method (FEM) is another common approach taken for simulating needle deflection (DiMaio & Salcudean, 2003; Alterovitz et al., 2005). DiMaio and Salcudean (2003), and Goksel et al. (2006) were amongst the first to use FEM to model the needle-tissue interaction. Initially, a FEM model was used to simulate deflection of a needle in free space and to take geometric nonlinearities into account (Goksel et al.,2009). To model the effects of surrounding tissue, a linear elastic tissue model was used. The geometry of the soft tissue is defined using a mesh composed of 2D or 3D polyhedral elements that are deformed as the needle cuts and advances into tissue (Gao et al., 2016). Alterovitz et al., (2005a, 2005b) incorporated the effects of the bevelled tip in the 2D FEM model in order to perform motion planning for steerable needles without the need for explicit position feedback (Alterovitz et al., 2009). Later, Chentanez et al. (2009) expanded the model to 3D. In Maghsoudi and Jahed, (2012a, 2012b), FEM is also used to estimate needle-tissue contact forces that result from tissue deformation. Similarly, in Dehghan and Salcudean (2009), a FEM-based model path planner takes into account the effects of boundary conditions, elasticity, and nonlinearity, in order to find the best path towards the updated location of a target. Then, a FEM-based feedback controller makes the needle follow the optimal path calculated online (Hauser et al., 2009).

Other applications of FEM include modelling the effect of external forces applied to the tissue in order to shift the target location and improve the needle targeting accuracy Torabi et al. (2009). Mallapragada, Sarkar, and Podder (2009) used this concept for breast biopsy procedures. It can also be used to enhance target accessibility by pushing obstacles and sensitive tissue away from the needle path.

Because of its high flexibility, FEM-based models can effectively describe the behaviour of needles in tissue in the presence of external perturbations. Employing such a comprehensive FEM model can be very time-consuming and not suitable for real-time control. More computationally efficient models may come at the expense of reduced accuracy (Goksel et al., 2006). Furthermore, certain parameters in FEM simulators may not relate to physical properties that can be experimentally and independently measured. In this regards, mechanics-based models can then be considered.

2.3. Mechanics-based models

To account for the fact that needle deflection and tissue deformation are coupled effects, researchers have adopted beam theories to develop fundamental mechanics-based models of needles in tissue (Asadian et al., 2011; Goksel et al., 2009; Khadem et al., 2015; Yan et al., 2009). Goksel et al. (2009) were amongst the first to develop mechanics-based models of a needle in free space subjected to a constant load applied at the tip. Tissue deformation is modelled by contact forces that evolve as the needle bends and compresses the tissue.

The Euler-Bernoulli equation describes the relationship between the beam's deflection v at a point z along its shaft and the applied load q as

$$\frac{d^2}{dz^2}\left(EI\frac{d^2v}{dz^2}\right) = q, \tag{2}$$

where EI is the needle's flexural rigidity, and q is a distributed load that acts anywhere along the needle shaft. Integrating both sides of (2) with respect to the position z gives the shear force acting on the needle. To the obtained shear force, the tip force Q is added and the result is further integrated until the deflection $v(t, z)$ is obtained. The key question in mechanics-based modelling is then how to model the distributed load q, and the needle tip force Q.

With regards to the vertical tip force Q, there are two main modelling approaches. Initially, the forces F, P, and Q were related to the geometry of the bevel edge and to the tissue properties, which suggested a constant, velocity-independent cutting force F (Abayazid et al., 2013; Mahvash & Dupont, 2010; Misra et al., 2008, 2010; Okamura et al., 2004). Nevertheless, it has been shown that model accuracy for a given insertion velocity decreases as the velocity changes (McGill et al., 2012; Podder et al., 2005). More recent models reported velocity-dependent fracture toughness at the needle tip (Barnett et al., 2016; Khadem et al., 2016; Maurin et al., 2004). Thus, the fact that the tissue acts as a low pass filter in response to fast needle insertion can be used to minimize tissue deformation and damage (Mahvash & Dupont, 2009; Lagerburg et al., 2006).

The distributed load q is typically calculated assuming that the tissue is a viscoelastic medium of stiffness K and viscous coefficient C that supports the needle shaft (see Figs. 4a and b). Typically, the distributed load q is assumed to have linear dependence on the

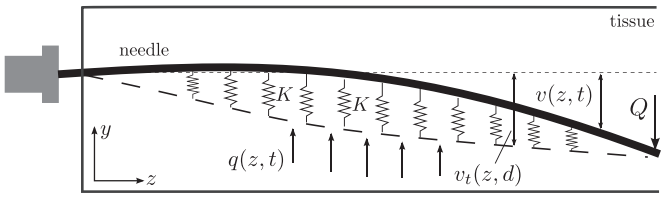

(a) Forces acting on the needle shaft

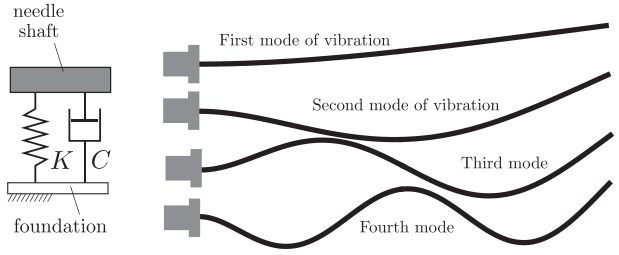

(b) Tissue (c) Vibration modes of a cantilever beam

Fig. 4. Mechanical-based model of needle-tissue interaction. In (a) the forces acting on the needle shaft are shown. Q is a the vertical component of the tissue cutting force, $q(z, t)$ is the force due to tissue deformation, $v(z, t)$ is the needle deflection, v_t is the trajectory of the needle tip, and K is the tissue stiffness. (b) shows the viscoelastic model of the tissue with a viscous coefficient C. In (c), the vibration modes of a cantilever beam are shown.

magnitude of deflection (Abayazid et al., 2013; DiMaio & Salcudean, 2003; Khadem et al., 2016, 2015; Misra et al., 2010; Moore et al., 2011). The stiffness K can either be fitted to the model for insertion lengths with constant bevel orientation, or assumed to be depth-dependent (Asadian et al., 2011; Yan et al., 2009, 2006). More recently, in Khadem et al. (2016a), Rossa et al. (2016a) and Rossa et al. (2017), the load q is found by considering the local magnitude of tissue deformation instead of that of needle deflection. The idea is that as the needle tip cuts through tissue, it creates a tunnel corresponding to the historical location of the needle tip ($v_t(t, z)$ in Fig. 4a). The local tissue deformation at point z is the difference between the position of the needle shaft at that location and the past position of the needle tip, i.e., $\delta = v(t, z) - v_t(t - \tau, L)$, where t is time, τ is a delay term, and L is the needle length. Thereby, it yields $q(z) = K\delta - C\dot{\delta}$. The partial differential equation (PDE) governing the motion of the needle can be written in the form

$$EI\frac{d^4v(t, z)}{dz^4} + c_1\frac{d^2v(t, z)}{dt^2} + P\frac{d^2v(t, z)}{dz^2} = Qu_3(t), \tag{3}$$

where c_1 is a constant that depends on the mechanical properties of the needle, and $u_3(t)$ is a step-type function that changes the sign of Q depending on the orientation of the bevel tip (rotation of the needle base), i.e., $u_3 = 1$ makes the needle deflect downwards, and $u_3 = -1$ makes the needle deflect upwards. This formulation automatically accounts for an unlimited number of needle axial rotations.

Note that in (2) the deflection $v(t, z)$ is both a function of position z and time t and thus the PDE given in (3) cannot be solved using conventional methods such as separation of variables (Khadem et al., 2015). The deflection is then approximated by a linear combination of n arbitrary candidate shape functions $W(z)$ representing the modes of vibration of a clamped-free beam (see Fig. 4c), that is

$$v(z, t) = \sum_{i=1}^{n} \Phi_i(t) W_i(z). \tag{4}$$

Here, $\Phi_i(t)$ are time-dependent eigenvalues to be determined such that the needle-tissue system reaches equilibrium, and n is the number of assumed vibration modes (Genta, 2009).

An energy-based formulation has been used to find the coefficients $\Phi_i(t)$ in Rossa et al. (2016a) and Rossa et al. (2017). In Abayazid et al. (2013) and Misra et al. (2010) the needle shape is approximated by a third order polynomial equation and a similar formulation is derived to find the polynomial coefficients. The model accounts for lateral and axial deflection of the needle, tissue deformation, and force applied at the needle base. Later, the same model was extended to include needle axial rotation during insertion (Roesthuis et al., 2012), and to model the behaviour of a needle in tissue when a permanent magnetic field applies forces to the needle shaft in an attempt to provide additional control over needle deflection (Datla et al., 2014).

Since the needle axial rotation is the main control command over deflection, its torsional dynamics can have an effect on steering accuracy (Swensen et al., 2014). Reed et al. (2009a, 2009b) studied the effects of torsional friction and compensated for it by a model-based controller.

Mechanics-based models require mechanical properties of the tissue as inputs, which can be obtained from direct measurement. Tissue parameters such as Young's modulus, tissue cutting force, and stiffness are commonly assumed to be constant throughout the insertion, or approximated by a series of different local finite homogeneous models (Lee and Kim, 2014). It has been shown such parametric mismatch can have drastic effects on steering accuracy (Maghsoudi & Jahed, 2012a, 2012b). Yet, most of the models reported above assume a homogeneous medium and model parameters. To account for modelling uncertainties, one may consider adaptive models.

2.4. Adaptive models

Given feedback from needle deflection, it is possible to evaluate model accuracy and adjust its parameters to best match observed measurements. The motivation behind adaptive models is that uncertainties arising from tissue heterogeneity, tissue deformation, needle buckling, tracks left in the tissue by previous insertions, and other unmodelled factors, can be accounted for to some extent (Rossa et al., 2016a; Yan et al., 2006).

Adaptive online identification of model parameters has been developed for both mechanics-based and nonholonomic kinematic models. A simple approach involves adding noise to the input parameters of an ideal model Park et al. (2005). Based on needle tip tracking information obtained from 2D axial ultrasound image slices, Carriere et al. (2016) used a particle filter to inform a kinematic model about the current location of the needle tip in order to create adaptive estimates of the radius of curvature κ in (1). It iteratively updates the parameters of (1) for each input ultrasound image frame and updates the predicted needle tip path. Along the same lines, Moreira and Misra (2015) proposes a method to update the needle curvature for use in closed-loop steering. The radius of curvature, initially empirically related to the tissue Young's modulus of elasticity, is updated online through a linear Kalman filter.

Adaptive models have also been proposed for mechanics-based approaches in order to update physical properties of either the needle or tissue. The authors in Yan et al. (2006) devised a model with depth-varying mean parameters that calculates the tissue stiffness K and viscosity C effects. As outlined in Rossa et al. (2016a), a needle model that updates the magnitude of the needle-tissue cutting force $Q(t, L)$ in (3) as the needle is inserted, can account for local variability in the tissue properties.

An alternative approach is to develop data-based methods to build a model of the plant from measurements of needle-tissue interactions Rossa et al. (2016). Such models can be a valuable solution to estimate the system output without deep understanding of the system physics. This is, however, beyond the scope of this paper.

3. Sensor for feedback control

Closed-loop feedback control requires real-time measurement of needle deflection. Typically, deflection is measured as close as possible to the needle tip using ultrasound images or alternative sensors such as optical fibres. The information is then fed back in the controller. Depending on the model employed, state estimation may also be necessary. In this section, we will review the issues related to sensing needle deflection during insertion.

3.1. Image-based feedback

Needle steering is often performed under ultrasound (US) image guidance. The literature on segmenting needles from ultrasound images is quite extensive. Here, we will only provide the reader with an overview of the main issues related to ultrasound image-based needle tracking. These are two steps, namely segmenting the needle from the image, and filtering out noise.

Three common imaging modalities are 3D volumetric ultrasound, 2D sagittal (longitudinal) imaging, and 2D transverse imaging (see Fig. 5). Sagittal ultrasound images (Fig. 5(a)) are acquired in a plane parallel to the needle's shaft and provide a consistent view of the needle from which the needle tip position can be obtained. However, depending on how the needle deflects, only a portion of the needle may be visible in the images (see Fig. 5a). Transverse images (Fig. 5(b)), on the other hand, are obtained in a plane perpendicular to the shaft and show a cross section of the needle, thereby eliminating complications of probe alignment at the cost of only seeing a single cross section of the needle along each transverse image (see Fig. 5b). 3D ultrasound images

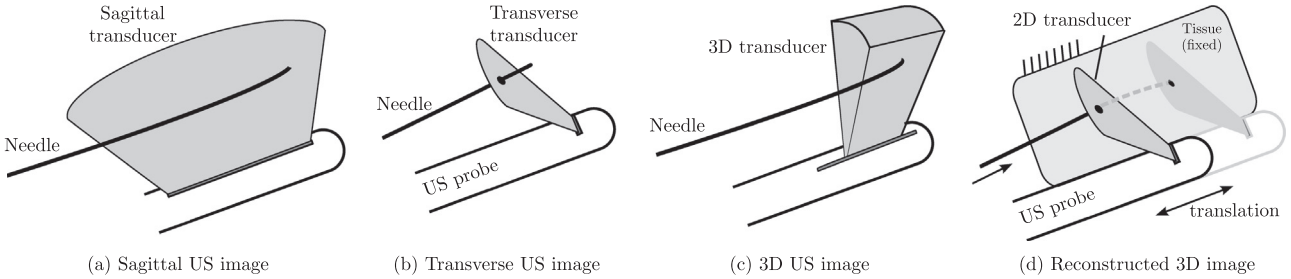

(a) Sagittal US image (b) Transverse US image (c) 3D US image (d) Reconstructed 3D image

Fig. 5. Classification of ultrasound image feedback for needle steering control. In (a), the 2D transverse image shows a cross section of the needle, in (b) the sagittal image aligns with the needle shaft, in (c) a volumetric probes builds a 3D image of the needle in tissue, and in (d) a 3D image is obtained from a series of 2D images.

(Fig. 5c) build a volumetric image of the tissue from crystal arrays pointing in different directions and fired in a particular sequence (Novotny et al., 2007). Other machines have a single 2D array of crystals that moves within the ultrasound probe in order to construct the 3D image from a set of 2D images Abayazid et al., 2016; Aboofazeli et al., 2009; Neshat & Patel, 2008). The field of view of such 3D transducers is often very narrow and thereby only a small portion of the needle can be visualized at a time. Although 3D imaging is expected to enlarge the sampled volume thereby increasing the accuracy of hitting a target (Long et al., 2007), typically only one to two 3D images can be reconstructed per second. This makes the modality not suitable for real-time control.

As an alternative to the above, the 3D path followed by the needle tip can be obtained from a series of 2D transverse images acquired at different depths in tissue (see Fig. 5d). In this case the ultrasound probe moves in synchrony with the needle, such that the same cross section of the needle is visible in the images. Recent techniques make use of motorized probes that move with the needle tip (Abayazid et al., 2014), or translate along the shaft once the needle is fully inserted (Carriere et al., 2015).

Another primary limitation in using ultrasound images is the low quality of images that often contain artifacts that are hard to interpret and distinguish from targets. Accurate localization of the needle in such noisy environment requires post-processing and filtering. Kaya and Bebek (2014) used Gabor filtering to estimate the insertion angle and minimize outliers while the needle trajectory is found with polynomial fit estimator. Other researches implemented needle tracking based on a Hough transform (Ding & Fenster, 2003; Okazawa et al., 2006; Qiu et al., 2008; Zhou et al., 2008) and Hough circle transform (Ayvali & Desai, 2014) in order to find highly bent needles in the images.

Linear Kalman filter has also been successfully used for needle tracking in ultrasound images to predict where the needle is within a region of interest (Chatelain et al., 2013; Vrooijink et al., 2014; Waine et al., 2016; Zhao et al., 2012). It is assumed that the needle is being inserted along the z axis as in Fig. 3(b), and axial ultrasound images are used to capture the needle tip position in the xy plane. If one looks at the needle tip as a point in the xy image, one can make the assumption that the frame-to-frame motion of the needle tip in the imaging plane is slow and so the linear Kalman filter is designed to reduce large quick changes in estimated needle tip position (corresponding to a low needle tip velocity in xy). These noise-reduced estimates are then input to a given needle steering controller without any change to the original needle-tissue model. For instance, Waine et al. (2016a) applied this concept to remove outliers such as those resulting from air bubbles and tissue inhomogeneity, which can often be mistaken for the needle's cross section when performing insertions into biological tissue.

In most of the above methods, the ultrasound probe must move in synchrony with the needle, which can result in further unwanted deformation of the tissue. Two options are then available. The first involves monitoring the location of the target and the motion of the surrounding tissue in real time (Dehghan et al., 2007, 2008; Hing et al., 2007; Klein et al., 2008; Long et al., 2012; Wei et al., 2004), and then compensating for any displacement in the control loop (Kojcev et al., 2016). The second option combines ultrasound images with a physical model of the needle in tissue, and relies only on the observation of a portion of the needle shaft for measuring its entire deflection. The latter is elaborated below.

3.2. Feedback from partial image observation

The idea of estimating the needle tip location based on partial image observation has been proposed in order to limit the motion of the ultrasound probe and minimize discrepancies between pre-and intra-operative target locations due to tissue displacement.

In Rossa et al. (2016), a method is proposed to predict needle deflection based on the observation of deflection from a single transverse image located along the needle shaft. The needle is modelled as a series of springs and rigid bars connected in series. The deflection measurement obtained from the transverse image is then used to determine the model parameters and estimate the *entire* needle shape. The ultrasound probe can be maintained at one fixed position as the needle is inserted. The method was later adapted to work with sagittal ultrasound images in Carriere et al. (2015). In Rossa et al. (2016a), the idea of partial image observation was further extended through a model that adaptively updates the needle-tissue contact forces as a function of the tissue displacement along the needle shaft. An ultrasound probe follows the needle tip and stops at an appropriate position while the needle is still being inserted. The model parameters are then adjusted such that the predicted deflection matches the measurement. Partial observation combined with the linear Kalman filter was used in Waine et al. (2016a) to determine optimal needle rotation depths that minimize targeting errors.

3.3. State observers

Consider a typical scenario where feedback of needle tip deflection (i.e., x, y, z in (1)) is obtained from 2D transverse ultrasound images. Since knowledge about the needle orientation (α, β, γ) is also necessary for prediction and control, model-based state observers can be employed to estimate non-measurable variables Asadian et al. (2011); Cowan et al. (2011); Fallahi et al. (2016).

Kallem and Cowan (2009) designed a linear observer for a kinematic model (Webster et al., 2006) in generalized coordinates such that from the information about needle tip, the needle pitch, roll, and yaw can be determined. This approach only requires the extraction of the needle tip position from images, rather than the entire needle shape, thereby simplifying the image segmentation problem. In Motaharifar et al. (2012), the observer is extended to work with a feedback linearisation controller. Similarly, a nonlinear observer that uses Cartesian position measurement data to estimate the orientation of the needle tip in tissue is described in Fallahi et al. (2016). The zero convergence of the observer error is shown using Lyapunov-based methods. Heverly et al. (2005) used a linear model to represent the dynamics of the unmeasured states via state immersion into a finite higher dimensional manifold. The observer estimates the complete needle orientation and also filters noisy position measurements.

Through the following state transformation of variables $s = [x, \sin(\beta), -\cos(\beta)\sin(\gamma)]^T$, (1) can be re-written in the form $\dot{s} = As + \phi(u, s)$, which outputs $y_{mes} = Cs = x$, where A is constant matrix and $\phi(u, s)$ is the non-linear component of the transformed system. From the measured deflection y_{mes}, one estimates the states of the transformed system as $\hat{s} = A\hat{s} + \phi(u, \hat{s}) + \Delta L(\hat{y} - y_{mes})$, where Δ is a diagonal constant matrix, and L is designed such that $A + LC$ is Hurwitz.

Disturbance observers can also be employed in the control of systems with external disturbances or model uncertainties (Park & Lee, 2007). In Maghsoudi and Jahed (2012), an FEM model of the tissue calculates the forces acting on the needle by considering them as external disturbances being applied to the needle.

3.4. Alternative sensors

As an alternative to imaging modalities such as ultrasound (Hong et al., 2004; ; Novotny et al., 2007; Rossa et al., 2016a, 2016b), X-Ray (Daly & Templeton, 1999; Gusmao et al., 2003; Kirkham, 2006; Pouliot, 2004; Turkbey, 2009; Van Sonnenberg, 1983), MRI (Anastasiadis et al., 2006; Kokes et al., 2009; Patriciu et al., 2007; Seifabadi et al., 2012; Susil, 2004), or fusion of MRI and ultrasound Xu et al. (2008), which are often limited in resolution and sampling rate, image-based feedback can be substituted with soft sensors.

An interesting concept to estimate deflection is to use a continuum robot as a force sensor and then estimate needle deflection using a mechanical model (Bajo & Simaan, 2010). In Xu and Simaan, (2008, 2010), Xu and Simaan demonstrated that by sensing loads on a continuum robot, certain components of the force applied at the end-effector can be determined. Rucker et al. (2011) extended this approach to estimate forces applied at the tip of a tendon-driven continuum robot using a kinematic model and uncertain pose measurements. Along the same lines, Abolhassani et al. (2007) introduced a force-sensor based estimator for needle deflection. Forces and torque measured at the needle base are related to the loads applied to the needle through (2). The concept is rather simple: Integrating once both sides of (2) gives the shear-force $F(z)$, and the integral of the shear force is the bending moment $M(z)$. When a force sensors is attached to the needle base, $F(z = 0)$ and $M(z = 0)$ are known at any time allowing one to solve for the model parameters q and Q. The needle deflection $v(t, z)$ is then calculated by further integrating the bending moment twice. The concept was further explored in Lehmann et al., (2015, 2016a, 2016b) in order to adaptively update the shape of loads acting on the needle. A model that accepts needle axial rotations based on this concept is yet to be developed. Longitudinal insertion force data has been also used for identifying tissue layers as the needle is inserted Abolhassani et al. (2007), which can help further enhance the force-based estimation proposed in Abolhassani et al. (2007) and Lehmann et al. (2015, 2016a, 2016b).

Fiber Bragg grating is another attractive alternative to sensing in the biomedical field due to advantageous properties (Al-Fakih et al., 2012) such as lower noise when compared to imaging. It has been demonstrated in Abayazid et al. (2013), Henken et al. (2012), Park et al. (2008) that an optical fiber embedded into the needle can be used for direct measurement of needle deflection, and even for three-dimensional reconstruction of the needle shape (Roesthuis et al., 2014).

4. Needle steering controller design

The next subsystem of our needle steering control scheme is the controller itself that, given the current information about needle deflection and, in some cases, the estimated future deflection, calculates the necessary steering actions that bring the needle on the desired trajectory.

Needle steering controllers can be classified into three main categories according the control objective, as illustrated in Fig. 6. The first and simplest controller aims at navigating the needle tip to a desired point in tissue. We will henceforth refer to this control problem as *weak regulation*. Two typical applications of weak regulation are tissue sampling (biopsy) (Baumann et al., 2012; Heidenreich et al., 2011; Lindgren, 1982) and percutaneous ablation (Morimoto et al., 2010; Solbiati et al., 1997), where the needle tip must move to a desired location regardless of what trajectory it takes. The second category comprises controllers whose control objective is to minimize the needle deflection at all depths. We will refer to this category as *regulation*. Applications of regulation can be found in transperineal prostate brachytherapy where the needle is controlled to follow a path as close as possible to a straight line such that strands of radioactive seeds can be deposited along the insertion path (Davis et al., 2012; Nag et al., 2004; Viswanathan et al., 2012). The last category is the *tracking* problem, where the needle tip follows a pre-defined trajectory that is not necessarily a straight line. It is typically employed in cases where the needle must be manoeuvred to avoid anatomical obstacles such as muscles, bones, or vessels (Patil & Alterovitz, 2010; Alterovitz et al., 2005; Lyons et al., 2010; Xu et al., 2009). In the following, we will address each control objective.

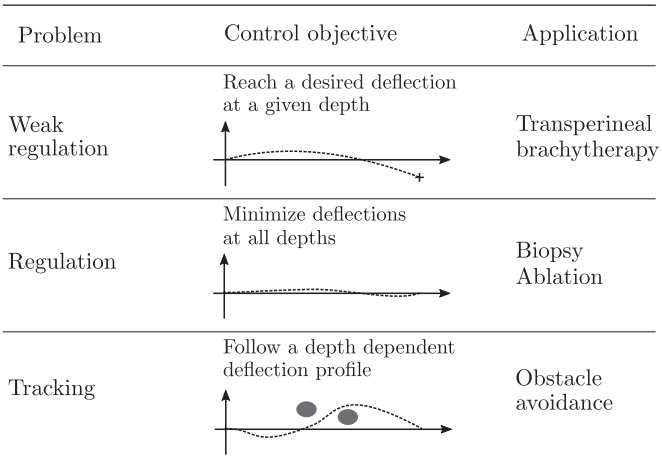

Fig. 6. Classification of needle steering controllers according to different control objectives.

4.1. Weak regulation

A weak regulator is often a model-based predictive controller. It is composed of a needle-tissue model and a solver that minimizes a cost function. The cost function typically relates different steering actions, i.e., twists or lateral motion of the needle shaft at different depths, to the model-predicted targeting error. The objective of the controller is to reach a desired target with a minimum amount of control actions such that tissue trauma is minimized. A popular choice for this purpose is the quadratic cost function

$$\Gamma(u) = \| x - x_{ref} \|^2 + \| y - y_{ref} \|^2 + \Lambda \| u_2 \|^2, \quad (5)$$

where $\|\cdot\|$ denotes the Euclidean norm, (x_{ref}, y_{ref}) is the reference trajectory, that is, a single point in case of weak regulation, and Λ is a weighing parameter that penalizes the control action.

The simplest weak regulator selects a single rotation depth that minimizes Γ, amongst a set of discrete rotation depth candidates, ranging from the current depth to the depth of the target (Lehmann et al., 2016). When more than one rotation is allowed, optimization of (5) needs a multi-variable and interactive solver. For instance, in Rossa et al. (2016), Rapidly-Exploring Random Three (RRT) is used. RRT incrementally grows a tree of feasible control actions, and provides a quick high dimensional search subject to different optimization constraints (LaValle, 1998; Bruce & Veloso, 2002). In Khadem et al.

(2016), a nonlinear Model Predictive Controller (MPC) iteratively optimizes (5) over a receding control horizon. The main difference between these approaches relies in the cost function and the selected iterative solver. Approaches such as Khadem et al. (2016) penalize both the predicted targeting error and steering actions, whereas Carriere et al. (2016), Lehmann et al. (2016) and Waine et al. (2016) define the control objective as having the smallest deviation from the target and do not restrict the control action ($\Lambda = 0$).

Other ways to minimize (5) involve solving for inverse kinematics models and create an optimal off-line path planning (DiMaio et al. 2005; Glozman & Shoham, 2007). A variety of algorithms are available for solving such optimization problems involving rigid bodies and articulated rigid bodies with kinematic and dynamic constraints (Latombe, 2012). Several motion planning algorithms have been used (Duindam et al., 2010; Park et al. 2009; Reed et al., 2011), including planning of 3D paths considering motion and sensing uncertainty. Researches have also combined online feedback obtained from needle tracking in ultrasound images such that the optimal depth of needle rotation can be updated online (Patil et al., 2014; Reed et al., 2008, 2009; Waine et al., 2016).

Generally speaking, the weak regulation control problem heavily relies on model accuracy. Alternative control methods are addressed in the next subsections.

4.2. Regulation

Regulation can be seen as a particular case of trajectory tracking where the reference trajectory is a straight line connecting the needle's entry point to the target point deep inside the tissue. The regulation error is, therefore, the measured deflection at all depths (see Fig. 6). Regulation problems are generally based on controllers such as sliding mode control, although predictive controllers have also been employed in an attempt to penalize the control action and minimize tissue trauma.

A common and intuitive approach in regulation is the continual duty-cycled rotation of the needle base (Engh et al., 2006, 2010; Majewicz et al. 2014; Minhas et al. 2007; Wood et al., 2010). When the needle is inserted without any change to the orientation of the bevel angle (no axial rotation of the needle base), the needle follows a trajectory with natural curvature κ. As the needle is inserted with constant twists of its base, at a rate relatively larger than its insertion velocity u_1, a trajectory close to a straight line can be achieved (Minhas et al., 2007). By combining periods of needle base rotation (T_{rot}) with periods of non-rotation (T), any curvature κ_d given by

$$\kappa_d = \kappa\left(1 - \frac{T_{rot}}{T_{rot} + T}\right), \tag{6}$$

ranging from the natural curvature κ to zero curvature can be achieved (Engh et al., 2006). The major limitation of this method arises from the tissue trauma and drilling effect generated by such periods of constant rotation.

Feedback linearisation of (1) is another common approach taken to regulate the needle to a single plane, namely the y, z plane (Kallem & Cowan, 2009). Let $r = [r_1, r_2, r_3]^T = [x, \beta, \gamma]^T$ denote the state vector of the reduced order system and r=0 be the desired equilibrium state. Through the state transformation $s = [r_1, \sin r_2, \kappa \cos r_2 \sin r_3]^T$ and $v = -\kappa^2 \sin r_2 + \kappa \cos r_2 \cos r_3 u_1$, the equation in the feedback linearized form is

$$\dot{s} = As + Bu_1 = \begin{bmatrix} 0 & 1 & 0 \\ 0 & 0 & 1 \\ 0 & 0 & 0 \end{bmatrix} s + \begin{bmatrix} 0 \\ 0 \\ 1 \end{bmatrix} u_1, \tag{7}$$

and $u_2 = Cs = [1, 0, 0]s$. This leads to a fully controllable and observable system. Recently, it has been shown that a similar controller can be derived using an integrator-backstepping approach (Waine et al., 2016). Let $\dot{r} = [\sin\beta, \kappa \sin\beta, -\kappa \cos\gamma \tan\beta]^T u_1 + [0, 0, 1]^T u_2$, and using the change of variable $\xi_1 = \sin\beta$ and $\xi_2 = \sin\gamma$, one can rewrite $\dot{r}$ in a strict feedback form. By controlling the needle to navigate around singularity points while switching regularly between two 2D integrator-backstepping controllers, it is possible to achieve 3D steering.

Inverse kinematics has been applied to regulation in Glozman and Shoham (2007, 2004), where a closed-loop control using X-ray imaging as feedback is designed based on a FEM model and a low-dimensional linear system of equations. Alternatively, a dynamic model of the needle-tissue system was proposed in Maghsoudi and Jahed (2012) and an inverse dynamics controller was designed. It showed that parametric mismatch can have drastic negative effects on the system behaviour and accuracy.

To minimize the effects of parameter mismatch, sliding model control for needle steering has been proposed (Fallahi et al., 2016; Rucker et al., 2013). Based on (1), a sliding mode control law independent of any model parameter is formulated in Fallahi et al. (2016) in 2D, and in 3D in Rucker et al. (2013), which allows for the model to reach any desired trajectory within a specified error. Considering only the deflection on the y, z plane, a common choice for the sliding surface is

$$s = c_2 \frac{de}{dt} + c_3 e \tag{8}$$

where $e = y_{ref} - y$ is the error from the desired trajectory, and c_2 and c_3 are positive defined constants. In a regulator, $y_{ref} = 0 \; \forall \; t$. When s exceeds a predefined threshold the needle is rotated by 180 degrees. The switching threshold is defined such that the orientation of the needle tip, i.e., α, remains bounded. Such controllers can be extended to follow any desired trajectory x_{ref}, y_{ref}, which brings us to the trajectory tracking problem.

4.3. Trajectory tracking

Trajectory tracking schemes are designed to use physician-selected and patient-specified parameters to define a path towards the target given the feasible needle insertion points, and locations of anatomical obstacles. Typically a trajectory tracking problem is implemented in two steps. The first step is preoperative. Based on the open-loop model, a motion planner determines a feasible path towards the target and the subsequent sequence of actions. The second part is intraoperative. The planned trajectory and/or the steering actions are updated online based on feedback of the needle tip (Cowan et al., 2011).

Tracking was initially proposed as a path planning algorithm in a 2D space with obstacles Alterovitz et al. (2005, 2008), and in an obstacle-free 3D environment (Park et al., 2005). Reed et al. (2008) combined a 2D planner with image feedback, a state observer, and the feedback linearized controller discussed in the previous section in order to compensate for out-of-plane deviations of the needle. In Minhas et al. (2007) and Majewicz et al. (2014), it is demonstrated that duty-cycle spinning can also be extended to follow arbitrary paths other than a straight line.

Since the 3D nonholonomic model has no closed-form solution in its original form (Webster et al., 2006), and, as we will see in Section 6, it is not possible to control such a 3D nonholonomic model using a smooth continuous control law, the control action is typically discretised and a multidimensional optimization solves for (5).

RRT optimization has been used in Rossa et al. (2016), Xu et al. (2008) and Patil and Alterovitz (2010) to deal with motion planning under nonholonomic constraints with discrete control input. Levenberg-Marquardt optimization is applied in Duindam et al. (2008) with a discrete controller whilst the path planning is solved algebraically. Path planning for such discrete control action is cast as a nonlinear optimization problem, which is solved via an analytic relation between position of the needle and control input. Researchers have also considered the effects of motion uncertainty and used Markov decision process to find optimal paths (Alterovitz

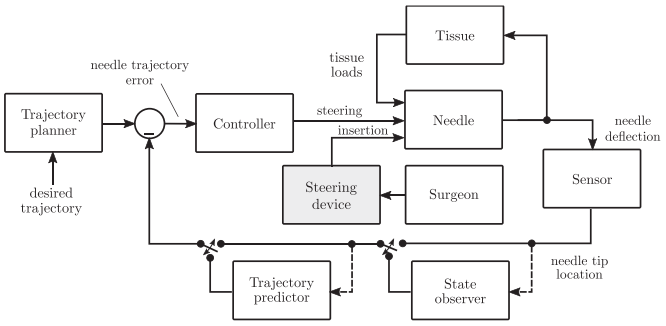

(a) Automation level 2 - Surgeon in-the-loop

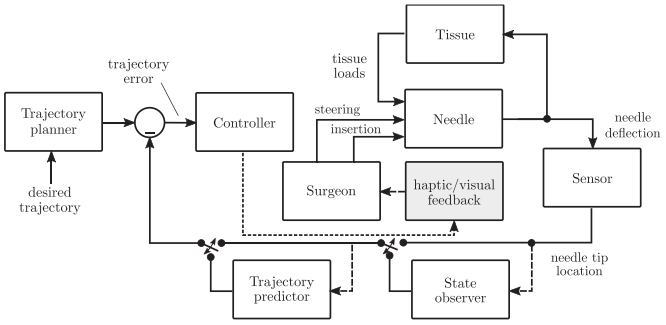

(b) Automation level 1 - Increasing surgeon awareness

Fig. 7. Other levels of automation of robotics-assisted needle steering. In (a), the robot steers the needle while the surgeon iserts it. In (b), the system simply informs the surgeon about necessary steering actions without intervening in the procedure.

et al., 2008, 2005), or replanned the reference trajectory online given the updated location of targets (Patil et al., 2014; Vrooijink et al., 2014).

In order to increase manoeuvrability around obstacles, modified needles such as notched (Khadem et al., 2016), and flexure-based steerable needles (Swaney et al., 2013) have been proposed. The idea is to modify the needle's flexural rigidify locally such that it follows a curvature that facilitates steering in constrained environments. Alternatively, pre-curved needles (Wedlick & Okamura, 2009) or those with actuated tip (Van de Berg et al., 2015) can also enhance steerability. These are only a few examples of regulation problems; many others can be found in the literature.

5. Needle steering robots

The last component of the closed-loop needle steering scheme is the steering device itself. Let us now turn our focus back to the starting point of our discussion, i.e., the system depicted in Fig. 1. Typically, two main control actions are used to steer the needle in combination with insertion, namely axial rotation of lateral forces applied at the needle base. The system we have considered so far is fully automated, meaning that the device performs both insertion and steering actions. There exists other levels of automation, i.e., semi-automated systems, where insertion is performed by the surgeon while steering occurs automatically (see Fig. 7a), and assisted manual steering, where the subsystems previously presented simply increase the surgeon's awareness about the procedure without explicitly intervening in it (see Fig. 7b). The role of the surgeon and of the robot in each of these scenarios is summarized in Table 1.

Table 1
The different varities of robotic needle steering according to their levels of automation.

Automation level	Operation modality	Surgeon's action	Machine action
0	fully manual	insertion/steering	none
1	assisted manual	insertion/steering	sensory feedback
2	semi automated	insertion only	steering only
3	fully automated	none	insertion/steering

5.1. Automation Level 3 - Fully automated steering

In this category the robot performs the insertion and all the steering actions (Adebar et al., 2011; Bassan et al., 2009; Hungr et al., 2012; Kobayashi et al., 2010; Long et al., 2012; Meltsner et al., 2007; Muntener et al., 2006; Neubach & Shoham, 2010; Patriciu et al., 2007; Phee et al., 2006; Podder et al., 2014; Shah et al., 2008; We et al., 2004; Wei et al., 2004; Yu et al., 2006) (as depicted in Fig. 1). Once the surgeon defines the insertion location, the desired target, and anatomical obstacles, the robotic system calculates a feasible path and steers the needle to the target.

Examples of fully automated needle steering systems include the backdrivable 5-DOF needle manipulator by Bassan et al. (2009), designed to orient the needle base and perform both insertion and rotation in prostate brachytherapy. A similar concept was adopted in Hungr et al. (2012) and Long et al. (2012) and combined with intraoperative prostate tracking. Wei et al. (2004) used a 6-DOF industrial robotic arm to orient and insert the needle while images of the target are acquired in 3D via a static volumetric ultrasound probe. MRI guidance (Muntener et al., 2006; Patriciu et al., 2007), and elastography (Adebar et al., 2011) have also been integrated with steering devices.

These robots replace the surgeon and are intended to make the motions and manoeuvres very precise, which may lead to better targeting accuracy when compared to traditional manual needle steering (Khadem et al., 2016). However, integrating these systems into current clinical practice is challenging and most often several modifications to the operating room are necessary. Anecdotally, one of the earliest medical robots and in fact the first ever to remove tissue from a patient falls in this category (Harris et al., 1997). It was used in transurethral resection of prostatic hyperplasia.

Fully-automated needle steering may represent a risk for the patient if the system becomes unstable. To manage this limitation, one can consider sharing needle insertion and steering actions between a physician and a robot, which leads to the second category of steering robots.

5.2. Automation Level 2 - Semi automated steering

In this category the robotic system acts as a needle holder that either rotates the needle axially or moves its base laterally with the physician being in charge of insertion (Bebek et al., 2013; Fichtinger et al., 2008; Hendrick et al., 2015; Salcudean et al., 2008; Schneider et al., 2004; Vitrani et al., 2016; We et al., 2004).

The latter concept has been introduced in Salcudean et al. (2008). The 4-DOF robot translates a needle guide in the x, y plane allowing for precise needle insertion along the z direction. It can also rotate the guide about the x and y axes, providing control over the needle insertion point and angle. Similarly, Kettenbach et al. (2005) developed a planar 2D needle holder that provides planar motion, through which the physician manually inserts the needle into the patient, thus retaining full control and natural haptic sensing. In Bebek et al. (2013), the needle manipulator has 5-DOF, allowing for angled insertions. Other applications of co-manipulation of either needles and/or ultrasound probes can be found in biopsy (Vitrani et al., 2016), and teleoperated schemes (Abolhassani & Patel, 2009; Goksel et al., 2011; Hing et al., 2006; Kokes et al., 2009; Nisky et al., 2011; Piccin et al., 2009; Seifabadi et al., 2012; Zarrad et al., 2007).

Moving away from fixed robotic structures, researchers have also considered hand-held devices (Hendrick et al., 2015; Khadem et al., 2016; Okazawa et al., 2005; Rossa et al., 2017). Reducing the complexity of the robotic scheme not only facilitates implementation in

a clinical scene, but also offers move dexterity and freedom to the surgeon. In Okazawa et al. (2005), a hand-held needle steering device actuates a stylet placed inside the shaft, changing the needle's natural curvature to achieve a desired steering direction. In Khadem et al. (2016) and Rossa et al. (2017), a hand-held apparatus for accurate steering in prostate brachytherapy is proposed to automatically rotate the needle as the surgeon manually inserts it. Such a system is compatible with contemporary operating room settings, leaving current practice intact.

5.3. Automation Level 1 - Assisted manual steering

In the third class of automation, the physician performs both the insertion and steering actions. This category combines models and controllers with a communication medium designed to provide relevant information about required steering manoeuvres. Hence, the surgeon is in full control of the procedures and may or may not perform the steering actions calculated by the control scheme (see Fig. 1). One can classify these systems into two main subcategories, namely, visual or tactile feedback devices.

In the first category, control actions are transmitted to the surgeon visually, for instance through augmented reality (Blackwell et al., 2000; Nikou et al., 2000); Weiss et al., 2011). The device projects onto the patient's skin reconstructed images of the inner body acquired from different medical imaging modalities, adding an extra layer of visual information on top of the perception of the real world in real time, making many surgical tasks simpler and safer for the surgeon. Therefore, it enhances the surgeon's ability to visualize needles and anatomical structures within the patient's body. Specific applications for needle guidance include arthrography (Fichtinger et al., 2005; Fischer et al., 2007) ultrasound guided needle placement training (Mageee et al., 2007), surgical laparoscopy (Nicolau et al., 2011), magnetic resonance guided biopsy (Wacker et al., 2006), liver puncture (Nicolau et al., 2005) and ablation (Nicolau et al., 2009; Teber et al., 2009), and computed tomography (Stetten & Chib, 2001; Stetten et al., 2001); Susil et al., 1999).

In the second subcategory, information is given to the surgeon in the form of tactile haptic feedback (Basu et al., 2016; Gerovich et al., 2004; Rossa et al., 2016). In Rossa et al. (2016), a wristband composed of several vibrating motors conveys haptic patters to inform about required steering manoeuvres such as needle rotation, needle base manipulation, acceleration, withdrawal etc. In Basu et al. (2016), haptic feedback on the arm provides intuitive movement cues to assist a human during needle insertion into the chest. Although implementing such assistants would only require minor modifications to the operating room, the outcomes still depend heavy on the operator's ability to perform steering actions.

6. Issues in closed-loop needle steering

The process of designing a closed-loop steering system involves the very same steps found in control systems generally. A typical scenario is as follows: study of the systems to be controlled, modelling, simplification, specification of performance, controller design, hardware implementation, controller tuning, and performance evaluation. Let us now discuss how each of these points fit in the context of needle steering schemes.

Studying the system to be controlled: In this step, one analyses all aspects of the medical procedure for which the system shall be designed. At this state, one must specify what types of sensors and actuators will be used and where they will be placed. Some applications only accept medical imaging as sensors, which comes at the cost of low sampling rate, poor image quality (particularity in the case of ultrasound), acquisition and processing delays, image registration uncertainty, and poor visualization of the task being performed. Sensorizing needles directly is the most reliable way of acquiring feedback on the tip position with the inconvenience of having to modify the clinical practice.

Modelling the system to be controlled: The second step involves identifying needle-tissue interaction models that are suitable as a basis for robust control design. There are several aspects to be considered in this regards. Firstly, such a model must be controllable, observable, and provide good control performance. Secondly, it must be fast enough to be run in real time. Thirdly, the model must be a good approximation of the real system and therefore needs to limit the upper bound on the mismatch between the plant and the identified model. Notwithstanding, none of the models we have discussed in Section 2 gather all of these features concurrently, not only because uncertainties such as tissue heterogeneity cannot be accurately accounted for, but also because FEM models are not suitable for real-time control, mechanics-based models are generally limited to 2D and in most cases are not useful for control, and no closed form solution can be obtained for the nonholonomic model expressed in 3D space nor can the tissue be modelled.

Let p_0 denote an equilibrium solution of (1) corresponding to $u_1 = u_2 = 0$. The following observations can be made about the model in (1):

1. The systems is nonholonomic, since the distribution closure is not involutive. Using successive Lie brackets, it can be shown that the system has nonholonomy degree of 4 and the rank of the system accessibility distribution is 6.
2. The system is driftless and affine in the inputs. Considering the accessibility rank, the system is strongly accessible controllable at p_0.
3. Based on Brockett's theory (Bloch et al., 2003; Brockett et al., 1983), a necessary condition for the existence a continuously differentiable control law that asymptomatically stabilises the system to p_0 is that there exists a neighbourhood N of p_0 such that for each $\epsilon \in N$ there exists a control $u = (u_1 u_2)$ defined $\forall\ t > 0$ that drives the states of (1) from $p = \epsilon$ at t=0 to $p = p_0$ as $t \to \infty$. The mapping

$$\begin{pmatrix} p \\ u_1 \\ u_2 \end{pmatrix} \to \begin{pmatrix} \sin(\beta)u_1 \\ -\cos(\beta)\sin(\alpha)u_1 \\ \cos(\alpha)\cos(\beta)u_1 \\ \kappa\cos(\gamma)\sec(\beta)u_1 \\ \kappa\sin(\gamma)u_1 \\ u_2 - \kappa\cos(\gamma)\tan(\beta)u_1 \end{pmatrix} \tag{9}$$

does not satisfy the Brockett condition. For instance, in the neighbourhood of $p_0 = [0, 0, 0, 0, 0, 0]$, where $0 < \beta < \pi$, no point in the format of $p = [0, \epsilon, 0, 0, 0, 0]$ exists. This means that the nonholonomic system in its full 3D form is not asymptotically stabilisable using continuous feedback law such as feedback linearisation, or any other control approach that uses smooth feedback. One can however stabilize to an equilibrium sub-manifold of the system via smooth feedback (Bloch et al., 1992), or use switching control to stabilize on an equilibrium point (Liberzon, 2003).

We have also seen that there are mainly two control actions i.e., needle rotation and shaft manipulation. A continuous model that unifies both inputs is yet to be developed.

Simplifying the model: Needle steering models are typically nonlinear, and in most of the cases, a closed form solution cannot be obtained unless some assumptions are made such as local linearisation, and small deflections (Fallahi et al., 2016; Khadem et al., 2016; Waine et al., 2016). This observation, however, goes against the previous point regarding model mismatch. The simplified model must still provide good accuracy while allowing for good control performance.

Specifying the desired performance: When referring to performance, one has to specify clearly what it means. In addition to desired outcomes such as robustness, disturbance rejection, fast convergence of tracking error, and accuracy, specific outcomes for needle based interventions involve minimizing any control effort that creates tissue

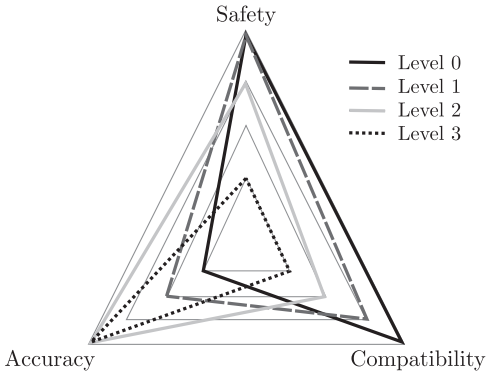

Fig. 8. The trade-off between safety, accuracy, and clinical compatibility for different levels of automation granted to needle steering robots. Automation level 0 corresponds to fully manual needle insertion and level 3 is fully automated.

trauma. Yet, it is clear that in regards to tissue trauma, those control objectives are contradictory, which reveals another trade-off in the design process.

Choosing the type of controller: When deciding on the type of controller to use, one must consider what signals it needs. For instance, some controller might require in addition to the position of the needle tip, measurement of the insertion velocity (Khadem et al., 2016), the orientation of the needle tip Fallahi et al. (2016); Waine et al. (2016), the deflection of the needle shaft (Khadem et al., 2016a, 2016b; Rossa et al., 2017, 2016), and/or the insertion force (Misra et al., 2010). Some of these measurements, however, cannot be obtained in certain applications of MIST. Other considerations concern robustness to intrinsic measurement noise, and control constraints. Depending on the desired performance and available measurements, one shall judiciously decide between predictive, sliding mode, duty-cycling approaches, or other methods.

Designing the controller: The next natural step consists in integrating the different parts that compose the needle steering system and implementing the controller. Depending on the hardware characteristics, control constrains must be addressed at this state such as imposing an upper bound on the insertion velocity and total rotation.

Designing the hardware and implementing the controller: We have classified the steering robots into three main categories depending on the degree of autonomy granted to it. A given controller requires a specific category of robots. For instance, a controller that modulates the needle insertion velocity should be used with a robot that takes over insertion (Khadem et al., 2016). Design considerations are also found in the range of Cartesian motion required to steer the needle, maximum insertion force and/or velocity, needle rotation capability, etc. It is also important to consider factors such as mechanical, electrical, and software failure, sterilization, operation, and safety (Fei et al., 2001). The latter is one of the key issues in designing a medical robot and implementing a controller. It can be addressed in many different ways ranging from the design of actuators to the use of redundant sensors.

Tuning the controller: Controller tuning refers to the selection of parameters to ensure satisfactory response. Adjusting the controller and the model parameters to a given tissue is essential to achieve good control performance. Choosing tuning that is too slow will result in slow response and convergence and the controller will not handle disturbances from the tissue. Choosing tuning that is too aggressive will create overshoots or lead the system to become unstable. As an example, one can consider the nonholonomic model that requires the radius curvature followed by the needle tip that varies from tissue to tissue and depends on the insertion depth (Fallahi et al., 2016). This directly influences the optimal control gains impacting the control effort and tissue trauma (Waine et al., 2016).

Evaluating system performance: Several indices characterize the controller and hardware performance. Typically it involves comparing the behaviour to some standard that, in the case of a medical robot, can be subjective. The most common measures of performance can be

Table 2
Non-exhaustive summary of documented needle steering controllers and systems.

Primary author	Model type[a]	2D or 3D	Position feedback	Control objective	Autom. level	Control action	Target error[b]
Smith et al. (2001)	(1)	3D	US images	regulation	3	rotation	0.27
Fichtinger et al. (2002)	n.a.	3D	CT images	regulation	2	shaft motion	1.00
Glozman & Shoham (2004)	FEM	2D	camera	tracking	3	base motion	–
Schneider et al. (2004)	n.a.	2D	US images	weak reg.	2	rotation	2.50
DiMaio et al. (2005)	FEM	2D	camera	tracking	3	base motion	1.00
Fichtinger et al. (2005)	n.a.	3D	CT images	weak reg.	1	base motion	2.00
Okazawa et al. (2005)	(2)	2D	camera	tracking	2	curvature	≈1.0
Phee et al. (2006)	FEM	3D	US images	regulation	2	base motion	2.50
Webster et al. (2006)	(1)	2D	camera	model[c]	3	rotation	1.30
Minhas et al. (2007)	(1)	2D	camera	model[c]	3	rotation	0.25
Bassan et al. (2009)	(1)	3D	US images	regulation	3	rotation	1.45
Dehghan & Salcudean (2009)	FEM	3D	US images	tracking	3	base motion	1.40
Kallem & Cowan (2009)	(1)	3D	camera	regulation	3	rotation	≈1.0
Kokes et al. (2009)	n.a.	3D	MRI	regulation	1	rotation	2.54
Maghsoudi & Jahed (2012)	(3)	2D	none	weak. reg.	3	n.a.	0.45
Abayazid et al. (2013)	(2)	2D	US images	weak reg.	3	rotation	0.46
Rucker et al. (2013)	(1)	3D	magnetic	weak reg.	3	rotation	0.43
Adebar et al. (2014)	(1)	3D	doppler	tracking	3	rotation	1.56
Patil et al. (2014)	(1)	3D	US images	tracking	3	rotation	2.38
Vrooijink et al. (2014)	(1)	2D	US images	tracking	3	rotation	0.86
Moreira & Misra (2015)	(1)	3D	US images	tracking	3	rotation	2.00
Fallahi et al. (2016)	(1)	2D	US images	regulation	3	rotation	0.55
Khadem et al. (2016)	(1)	2D	US images	tracking	2	rotation	1.22
Khadem et al. (2016)	(3)	2D	US images	regulation	3	rotation	1.45
Waine et al. (2016)	(1)	2D	US images	regulation	3	rotation	0.70
Rossa et al. (2017)	(2)	2D	US images	weak reg.	2	rotation	0.44
						Average	1.22

[a] Needle-tissue model formulation: (1) kinematic as in Eq. (1), (2–3) mechanical as in (2) or (3).
[b] Error is given in millimetres.
[c] Paper presents a model only

attributed to process variance (repeatability in reaching the target), set-point accuracy (accuracy in reaching the target), and minimization of the control effort (related to the effect on the surrounding tissue). If the resultant closed-loop system does not meet the specified standard, the design steps presented above can be reconsidered iteratively.

The highlighted trade-off in the design of steering robots translate into Fig. 8. Finding a good equilibrium between accuracy, patient safety, and compatibility with the clinical scene is still an open challenge that one can address in each of the design steps considered here. A variety of combinations of needle-tissue interaction models, deflection measurement modalities, and steering controllers have been proposed in order to best respond to the design requirements listed above, some of which can be seen in Table 2.

7. Concluding remarks

In this paper, we reviewed progress made in closed-loop needle steering control. We addressed various aspects that must be considered when implementing such systems, namely modelling of needle-tissue interaction, sensing needle deflection during insertion, implementing the controller, developing the hardware and evaluating the obtained performance.

Despite significant research effort on the subject during the past 15 years that has led to a solid average in reaching targets of about 1.22 mm (see Table 2), to date there is no commercially available solution for robotics-assisted needle steering. The limitations highlighted in this paper suggest that automated needle steering will not be widespread in the clinical scene until technological and clinical limitations related to modelling and control of needle steering are overcome. Hence, robust robotics-assisted needle steering remains to date an open challenge with considerable room for improvement.

One classic example that clearly highlights the potential benefits of accurate needle steering can be found in prostate brachytherapy. Due to the currently limited accuracy of manual steering (about 5 mm (Jamaluddin et al., 2017)), brachytherapy has been limited to primarily overtreating the entire prostate even for patients with only localized prostate cancer. Improving needle targeting accuracy by means of robotic assistance can result in enhanced treatment of localized prostate cancer and, in addition, make this treatment applicable to other clinical situations (Bott et al., 2010; Karavitakis et al., 2011). Accurate needle steering can also lead to more precise tissue biopsy, pinpoint drug deliver, improved ablation of lung, liver and kidney, access to deep zones in the brain, amongst many other benefits in general applications of MIST.

References

Abayazid, M. et al. (2013). 3D flexible needle steering in soft-tissue phantoms using fiber bragg grating sensors. In *Proceedings of IEEE international conference on robotics and automation*, pp. 5843–5849.

Abayazid, M. et al. (2013). Integrating deflection models and image feedback for real-time flexible needle steering. *IEEE Transactions on Robotics*, *29*(2), 542–553.

Abayazid, M. et al. (2014). Experimental evaluation of ultrasound-guided 3D needle steering in biological tissue. *International Journal of Computer Assisted Radiology and Surgery*, *9*(6), 931–939.

Abayazid, M. et al. (2016). Three-dimensional needle steering using automated breast volume scanner (ABVS). *Journal of Medical Robotics Research*, *1*(*01*), 1640005.

Abolhassani, N., & Patel, R. (2009). Teleoperated master-slave needle insertion. *The International Journal of Medical Robotics and Computer Assisted Surgery*, *5*(4), 398–405.

Abolhassani, N. et al. (2007). Minimization of needle deflection in robot-assisted percutaneous therapy. *The International Journal of Medical Robotics and Computer Assisted Surgery*, *3*(2), 140–148.

Abolhassani, N. et al. (2007). Needle insertion into soft tissue: A survey. *Medical Engineering & Physics*, *29*(4), 413–431.

Aboofazeli, M. et al. (2009). A new scheme for curved needle segmentation in three-dimensional ultrasound images. In *Proceedings of IEEE international symposium on biomedical imaging: from nano to macro*, pp. 1067–1070.

Adebar, T. et al. (2011). A robotic system for intra-operative trans-rectal ultrasound and ultrasound elastography in radical prostatectomy In: et al.(Ed.), Information processing in computer-assisted interventions. Springer, pp. 79–89.

Adebar, T. et al. (2014). 3D ultrasound-guided robotic needle steering in biological tissue. *IEEE Transactions on Biomedical Engineering*, *61*(*12*), 2899–2910.

Advincula, A., & Song, A. (2007). The role of robotic surgery in gynecology. *Current Opinion in Obstetrics and Gynecology*, *19*(4), 331–336.

Al-Fakih, E. et al. (2012). The use of fiber bragg grating sensors in biomechanics and rehabilitation applications: The state-of-the-art and ongoing research topics. *Sensors*, *12*(*10*), 12890–12926.

Alterovitz, R. et al. (2005). Planning for steerable bevel-tip needle insertion through 2D soft tissue with obstacles. In *Proceedings of* ieee international conference on robotics and automation, pp. 1640–1645.

Alterovitz, R. et al. (2005). Steering flexible needles under markov motion uncertainty. In *Proceedings of IEEE/RSJ international conference on intelligent robots and systems*, pp. 1570–1575.

Alterovitz, R. et al. (2008). Constant-curvature motion planning under uncertainty with applications in image-guided medical needle steering. In *Algorithmic Foundation of Robotics VII*, pp. 319–334, Springer.

Alterovitz, R. et al. (2008). Motion planning under uncertainty for image-guided medical needle steering. *The International Journal of Robotics Research*, *27*(*11–12*), 1361–1374.

Alterovitz, R. et al. (2009). Sensorless motion planning for medical needle insertion in deformable tissues. *IEEE Transactions on Information Technology in Biomedicine*, *13*(*2*), 217–225.

Anastasiadis, A. et al. (2006). MRI-guided biopsy of the prostate increases diagnostic performance in men with elevated or increasing psa levels after previous negative trus biopsies. *European Urology*, *50*(*4*), 738–749.

Asadian, A. et al. (2011). A distributed model for needle-tissue friction in percutaneous interventions. In *Proceedings of IEEE international conference on robotics and automation*, pp. 1896–1901, May.

Asadian, A. et al. (2011). An analytical model for deflection of flexible needles during needle insertion. In *Proceedings of IEEE/RSJ international conference on intelligent robots and systems* , pp. 2551–2556.

Asadian, A. et al. (2011). A distributed model for needle-tissue friction in percutaneous interventions. In *Proceedings of IEEE international conference on robotics and automation*, pp. 1896–1901.

Ayvali, E. & Desai, J. (2014). Accurate in-plane and out-of-plane ultrasound-based tracking of the discretely actuated steerable cannula. In *Proceedings of IEEE international conference on robotics and automation*, pp. 5896–5901.

Bajo, A. & Simaan, N. (2010). Finding lost wrenches: Using continuum robots for contact detection and estimation of contact location. In *Proceedings of IEEE international conference on robotics and automation*, pp. 3666–3673.

Barnett, A. et al. (2016). Fracture mechanics model of needle cutting tissue. *Journal of Manufacturing Science and Engineering*, *138*(*1*), 011005.

Bassan, H. et al. (2009). A novel manipulator for percutaneous needle insertion: Design and experimentation. *IEEE/ASME Transactions on Mechatronics*, *14*(*6*), 746–761.

Basu, S. et al. (2016). Evaluation of tactile guidance cue mappings for emergency percutaneous needle insertion. In *Proceedings of IEEE haptics symposium*, pp. 106–112, April.

Baumann, M. et al. (2012). Prostate biopsy tracking with deformation estimation. *Medical Image Analysis*, *16*(*3*), 562–576.

Bebek, O. et al. (2013). Design of a parallel robot for needle-based interventions on small animals. *IEEE/ASME Transactions on Mechatronics*, *18*(*1*), 62–73.

Blackwell, M. et al. (2000). An image overlay system for medical data visualization. *Medical Image Analysis*, *4*(*1*), 67–72.

Bloch, A. et al. (1992). Control and stabilization of nonholonomic dynamic systems. *IEEE Transactions on Automatic Control*, *37*(*11*), 1746–1757.

Bloch, A. et al. (2003). *Nonholonomic mechanics and control*, vol. 24. Springer.

Boctor, E. et al. (2004). A dual-armed robotic system for intraoperative ultrasound guided hepatic ablative therapy: a prospective study. In *Proceedings of IEEE international conference on robotics and automation* , vol. 3, pp. 2517–2522.

Bott, S. et al. (2010). The index lesion and focal therapy: An analysis of the pathological characteristics of prostate cancer. *BJU International*, *106*(*11*), 1607–1611.

Bowthorpe, M., & Tavakoli, M. (2016). Generalized predictive control of a surgical robot for beating-heart surgery under delayed and slowly-sampled ultrasound image data. *IEEE Robotics and Automation Letters*, *1*, 892–899.

Bowthorpe, M. et al. (2014). Smith predictor-based robot control for ultrasound-guided teleoperated beating-heart surgery. *IEEE Journal of Biomedical and Health Informatics*, *18*, 157–166.

Brockett, R. W. et al. (1983). Asymptotic stability and feedback stabilization. *Differential Geometric Control Theory*, *27*(*1*), 181–191.

Bruce, J. & Veloso, M. (2002). Real-time randomized path planning for robot navigation. In *Proceedings of IEEE/RSJ international conference on intelligent robots and systems*, vol. 3, pp. 2383–2388.

Carriere, J. et al. (2015). Needle shape estimation in soft tissue based on partial ultrasound image observation. In *Proceedings of IEEE international conference on robotics and automation*, pp. 2277–2282.

Carriere, J. et al. (July 2016). Real-time needle shape prediction in soft-tissue based on image segmentation and particle filtering. In *Proceedings of IEEE/ASME international conference on advanced intelligent mechatronics*, pp. 1204–1209.

Chapman, W. et al. (2001). Robotic nissen fundoplication: Alternative surgical technique for the treatment of gastroesophageal reflux disease. *Journal of Laparoendoscopic & Advanced Surgical Techniques*, *11*(*1*), 27–30.

Chatelain, P. et al. (2013). Real-time needle detection and tracking using a visually servoed 3D ultrasound probe. In *Proceedings of IEEE international conference on robotics and automation*, , pp. 1676–1681.

Chentanez, N. et al. (2009). *Interactive simulation of surgical needle insertion and steering*, vol. 28. ACM.

Cowan, N. et al. (2011). *Robotic needle steering: Design, modeling, planning, and image guidance. In Surgical Robotics*. Springer, 557–582.
Daly, B., & Templeton, P. (1999). Real-time CT fluoroscopy: Evolution of an interventional tool 1. *Radiology*, *211*(*2*), 309–315.
Datla, N. et al. (2014). A model to predict deflection of bevel-tipped active needle advancing in soft tissue. *Medical Engineering & Physics*, *36*(*3*), 285–293.
Davis, B. et al. (2012). American brachytherapy society consensus guidelines for transrectal ultrasound-guided permanent prostate brachytherapy. *Brachytherapy*, *11*(*1*), 6–19.
Dehghan, E., & Salcudean, S. (2009). Needle insertion parameter optimization for brachytherapy. *IEEE Transactions on Robotics*, *25*(*2*), 303–315.
Dehghan, E. et al. (2007). Modeling of needle-tissue interaction using ultrasound-based motion estimation. In *Proceedings of international conference on medical image computing and computer-assisted intervention*, pp. 709–716.
Dehghan, E. et al. (2008). Needle-tissue interaction modeling using ultrasound-based motion estimation: Phantom study. *Computer Aided Surgery*, *13*(*5*), 265–280.
Di Biase, L. et al. (2009). Ablation of atrial fibrillation utilizing robotic catheter navigation in comparison to manual navigation and ablation: Single-center experience. *Journal of cardiovascular electrophysiology*, *20*(*12*), 1328–1335.
DiMaio, S. & Salcudean, S. (2003). Needle steering and model-based trajectory planning. In *Proceedings of international conference on medical image computing and computer-assisted intervention*, pp. 33–40.
DiMaio, S. et al. (2005). Needle steering and motion planning in soft tissues. *IEEE Transactions on Biomedical Engineering*, *52*(*6*), 965–974.
Ding, M., & Fenster, A. (2003). A real-time biopsy needle segmentation technique using hough transform. *Medical Physics*, *30*(*8*), 2222–2233.
Duindam, V. et al. (2008). Screw-based motion planning for bevel-tip flexible needles in 3D environments with obstacles. In *Proceedings of IEEE international conference on robotics and automation*, pp. 2483–2488.
Duindam, V. et al. (2010). Three-dimensional motion planning algorithms for steerable needles using inverse kinematics. *The International Journal of Robotics Research*, *29*(*7*), 789–800.
Engh, J. et al. (April 2006). Flexible needle steering system for percutaneous access to deep zones of the brain. In *IEEE Proceedings of the 32nd annual northeast bioengineering conference*, pp. 103–104.
Engh, J. et al. (2010). Percutaneous intracerebral navigation by duty-cycled spinning of flexible bevel-tipped needles. *Neurosurgery*, *67*(*4*), 1117–1123.
Falcone, T., & Bedaiwy, M. (2002). Minimally invasive management of uterine fibroids. *Current Opinion in Obstetrics and Gynecology*, *14*(*4*), 401–407.
Fallahi, B. et al. (2015). Extended bicycle model for needle steering in soft tissue. In *Proceedings of IEEE/RSJ* international conference on intelligent robots and systems, pp. 4375–4380.
Fallahi, B. et al. (2016). Sliding-based switching control for image-guided needle steering in soft tissue. *IEEE Robotics and Automation Letters*, *1*, 860–867.
Fallahi, B. et al. (July 2016). Partial estimation of needle tip orientation in generalized coordinates in ultrasound image-guided needle insertion. In *Proceedings of IEEE/ASME international conference on advanced intelligent mechatronics*, pp. 1604–1609.
Fei, B. et al. (2001). The safety issues of medical robotics. *Reliability Engineering & System Safety*, *73*(*2*), 183–192.
Fichtinger, G. et al. (2002). System for robotically assisted prostate biopsy and therapy with intraoperative ct guidance. *Academic Radiology*, *9*(*1*), 60–74.
Fichtinger, G. et al. (2005). Image overlay guidance for needle insertion in ct scanner. *IEEE Transactions on Biomedical Engineering*, *52*(*8*), 1415–1424.
Fichtinger, G. et al. (2008). Robotic assistance for ultrasound-guided prostate brachytherapy. *Medical Image Analysis*, *12*(*5*), 535–545.
Fischer, G. et al. (2007). Mri image overlay: Application to arthrography needle insertion. *Computer Aided Surgery*, *12*(*1*), 2–14.
Gao, D. et al. (2016). Modeling and simulation of flexible needle insertion into soft tissue using modified local constraints, Journal of Manufacturing Science and Engineering.
Gayle, R. et al. (2005). Path planning for deformable robots in complex environments. *Robotics: Science and Systems*, *2005*, 225–232.
Genta, G. (2009). *Vibration dynamics and control*. Springer.
Gerovich, O. et al. (2004). The effect of visual and haptic feedback on computer-assisted needle insertion. *Computer Aided Surgery*, *9*(*6*), 243–249.
Gill, R. et al. (2011). Robotic-assisted bariatric surgery: A systematic review. *The International Journal of Medical Robotics and Computer Assisted Surgery*, *7*(*3*), 249–255.
Giulianotti, P. et al. (2010). Robot-assisted laparoscopic pancreatic surgery: single-surgeon experience. *Surgical Endoscopy*, *24*(*7*), 1646–1657.
Glozman, D. & Shoham, M. (2004). Flexible needle steering and optimal trajectory planning for percutaneous therapies. In *Proceedings of International Conference on Medical Image Computing and Computer-Assisted Intervention*, pp. 137–144.
Glozman, D., & Shoham, M. (2007). Image-guided robotic flexible needle steering. *IEEE Transactions on Robotics*, *23*(*3*), 459–467.
Goksel, O. et al. (2006). 3D simulation of needle-tissue interaction with application to prostate brachytherapy. *Computer Aided Surgery*, *11*(*6*), 279–288.
Goksel, O. et al. (2009). Modeling and simulation of flexible needles. *Medical Engineering & Physics*, *31*(*9*), 1069–1078.
Goksel, O. et al. (2011). Haptic simulator for prostate brachytherapy with simulated needle and probe interaction. *IEEE Transactions on Haptics*, *4*(*3*), 188–198.
Grimson, E. et al. (1996). An automatic registration method for frameless stereotaxy, image guided surgery, and enhanced reality visualization. *IEEE Transactions on Medical Imaging*, *15*(*2*), 129–140.
Gusmao, S. et al. (2003). Percutaneous trigeminal nerve radiofrequency rhizotomy guided by computerized tomography fluoroscopy: Technical note. *Journal of Neurosurgery*, *99*(*4*), 785–786.
Haddadi, A. et al. (2010). On the controllability of dynamic model-based needle insertion in soft tissue. In *Proceedings of annual international conference of the IEEE engineering in medicine and biology*, pp. 2287–2291.
Harris, S. et al. (1997). The probot-an active robot for prostate resection, Proceedings of the Institution of Mechanical Engineers, Part H: Journal of Engineering in Medicine, vol. 211, no. 4, pp. 317–325.
Hauser, K. et al. (2009). Feedback control for steering needles through 3D deformable tissue using helical paths, Robotics science and systems: online proceedings, p. 37.
Heidenreich, A. et al. (2011). EAU guidelines on prostate cancer. part 1: Screening, diagnosis, and treatment of clinically localised disease. *European Urology*, *59*(*1*), 61–71.
Hendrick, R. et al. (2015). Hand-held transendoscopic robotic manipulators: A transurethral laser prostate surgery case study. *The International Journal of Robotics Research*, *34*(*13*) (0278364915585397).
Henken, K. et al. (2012). Accuracy of needle position measurements using fiber bragg gratings. *Minimally Invasive Therapy & Allied Technologies*, *21*(*6*), 408–414.
Heverly, M. et al. (2005). Trajectory optimization for dynamic needle insertion. In *Proceedings of IEEE international conference on robotics and automation*, pp. 1646–1651.
Hing, J. et al. (May 2006). Reality-based needle insertion simulation for haptic feedback in prostate brachytherapy. In *Proceedings of IEEE international conference on robotics and automation* , pp. 619–624.
Hing, J. et al. (2007). A biplanar fluoroscopic approach for the measurement, modeling, and simulation of needle and soft-tissue interaction. *Medical Image Analysis*, *11*(*1*), 62–78.
Hong, J. et al. (2004). An ultrasound-driven needle-insertion robot for percutaneous cholecystostomy. *Physics in Medicine and Biology*, *49*(*3*), 441.
Horgan, S. et al. (2002). Robotic-assisted laparoscopic donor nephrectomy for kidney transplantation. *Transplantation*, *73*(*9*), 1474–1479.
Hungr, N. et al. (2012). A 3D ultrasound robotic prostate brachytherapy system with prostate motion tracking. *IEEE Transactions on Robotics*, *28*(*6*), 1382–1397.
Jamaluddin, M. et al. (2017). Quantifying 125-I placement accuracy in prostate brachytherapy using postimplant transrectal ultrasound images, Brachytherapy.
Kallem, V., & Cowan, N. (2009). Image guidance of flexible tip-steerable needles. *IEEE Transactions on Robotics*, *25*(*1*), 191–196.
Kang, S. et al. (2009). Robot-assisted endoscopic surgery for thyroid cancer: Experience with the first 100 patients. *Surgical Endoscopy*, *23*(*11*), 2399–2406.
Karavitakis, M. et al. (2011). Histological characteristics of the index lesion in whole-mount radical prostatectomy specimens: Implications for focal therapy. *Prostate Cancer and Prostatic Diseases*, *14*(*1*), 46–52.
Kataoka, H. et al. (2001). A model for relations between needle deflection, force, and thickness on needle penetration. In *Proceedings of international conference on medical image computing and computer-assisted intervention*, pp. 966–974.
Kaya, M. & Bebek, O. (2014). Needle localization using gabor filtering in 2D ultrasound images. In IEEE International Conference on Robotics and Automation, pp. 4881–4886.
Keereweer, S. et al. (2011). Optical image-guided surgery - where do we stand*. *Molecular Imaging and Biology*, *13*(*2*), 199–207.
Kettenbach, J. et al. (2005). Robot-assisted biopsy using ultrasound guidance: Initial results from in vitro tests. *European radiology*, *15*(*4*), 765–771.
Khadem, M. et al. (2015). A mechanics-based model for simulation and control of flexible needle insertion in soft tissue. In *Proceedings of IEEE international conference on robotics and automation*, pp. 2264–2269.
Khadem, M. et al. (2016). Introducing notched flexible needles with increased deflection curvature in soft tissue. In *Proceedings of* IEEE/ASME international conference onadvanced intelligent mechatronics, pp. 1186–1191.
Khadem, M. et al. (2016). Semi-automated needle steering in biological tissue using an ultrasound-based deflection predictor. *Annals of Biomedical Engineering*, 1–15.
Khadem, M. et al. (2016). A two-body rigid/flexible model of needle steering dynamics in soft tissue. *IEEE/ASME Transactions on Mechatronics*, *21*, 2352–2364.
Khadem, M. et al. (2016). Ultrasound-guided model predictive control of needle steering in biological tissue. *Journal of Medical Robotics Research*, *1*(*01*), 1640007.
Khadem, M. et al. (2016). Mechanics of tissue cutting during needle insertion in biological tissue. *IEEE Robotics and Automation Letters*, *1*, 800–807.
Kim, M. et al. (2010). Robotic gastrectomy for gastric cancer: Surgical techniques and clinical merits. *Surgical Endoscopy*, *24*(*3*), 610–615.
Kirkham, A. et al. (2006). How good is MRI at detecting and characterising cancer within the prostate*. *European Urology*, *50*(*6*), 1163–1175.
Klein, S. et al. (2008). Automatic segmentation of the prostate in 3D MR images by atlas matching using localized mutual information. *Medical Physics*, *35*(*4*), 1407–1417.
Kobayashi, Y. et al. (2010). Development of an integrated needle insertion system with image guidance and deformation simulation. *Computerized Medical Imaging and Graphics*, *34*(*1*), 9–18.
Kojcev, R. et al. (2016). Dual-robot ultrasound-guided needle placement: Closing the planning-imaging-action loop. *International Journal of Computer Assisted Radiology and Surgery*, 1–9.
Kokes, R. et al. (2009). Towards a teleoperated needle driver robot with haptic feedback for RFA of breast tumors under continuous MRI. *Medical Image Analysis*, *13*(*3*), 445–455.
Lagerburg, V. et al. (2006). Development of a tapping device: A new needle insertion method for prostate brachytherapy. *Physics in Medicine and Biology*, *51*(*4*), 891.
Lanfranco, A. et al. (2004). Robotic surgery: A current perspective. *Annals of Surgery*, *239*(*1*), 14–21.
Latombe, J. (2012). *Robot motion planning*, vol. 124. Springer Science & Business Media.

LaValle, S. M. (1998). Rapidly-exploring random trees: A new tool for path planning.
Lee, H., & Kim, J. (2014). Estimation of flexible needle deflection in layered soft tissues with different elastic moduli. *Medical & Biological Engineering & Computing*, *52*(*9*), 729–740.
Lehmann, T. et al. (2015). A virtual sensor for needle deflection estimation during soft-tissue needle insertion. In *Proceedings of IEEE international conference on robotics and automation*, pp. 1217–1222.
Lehmann, T. et al. (2016). Needle path control during insertion in soft tissue using a force-sensor-based deflection estimator. In *Proceedings of IEEE/ASME international conference on advanced intelligent mechatronics*, pp. 1174–1179.
Lehmann, T. et al. (2016). A real-time estimator for needle deflection during insertion into soft tissue based on adaptive modeling of needle-tissue interactions. *IEEE/ASME Transactions on Mechatronics*, *21*, 2601–2612.
Liberzon, D. (2003). Systems not stabilizable by continuous feedback. , in: *Switching in Systems and Control*. Springer, 77–91.
Lindgren, P. (1982). Percutaneous needle biopsy. A new technique. *Acta Radiologica: Diagnosis*, *23*(*6*), 653.
Long, J. et al. (2007). Prostate biopsies guided by three-dimensional real-time (4D) transrectal ultrasonography on a phantom: Comparative study versus two-dimensional transrectal ultrasound-guided biopsies. *European Urology*, *52*(*4*), 1097–1105.
Long, J. et al. (2012). Development of a novel robot for transperineal needle based interventions: Focal therapy, brachytherapy and prostate biopsies. *The Journal of Urology*, *188*(*4*), 1369–1374.
Luketich, J. et al. (2003). Minimally invasive esophagectomy: Outcomes in 222 patients. *Annals of Surgery*, *238*(*4*), 486–495.
Lyons, L. et al. (2010). Planning active cannula configurations through tubular anatomy. In *Proceedings of IEEE international conference on robotics and automation*, pp. 2082–2087.
Mageee, D. et al. (2007). An augmented reality simulator for ultrasound guided needle placement training. *Medical & Biological Engineering & Computing*, *45*(*10*), 957–967.
Maghsoudi, A. & Jahed, M. (2012). A comparison between disturbance observer-based and model-based control of needle in percutaneous applications. In *Proceedings of annual conference on IEEE industrial electronics society*, pp. 2104–2108.
Maghsoudi, A. & Jahed, M. (2012). Inverse dynamics control of needle in prostate brachytherapy. In *Proceedings of IEEE international conference on industrial technology*, pp. 510–515.
Maghsoudi, A. & Jahed, M. (2012). Model based needle control in prostate percutaneous procedures, Proceedings of the Institution of Mechanical Engineers, Part H: Journal of Engineering in Medicine, p. 0954411912458489.
Maghsoudi, A., & Jahed, M. (2012). Needle dynamics modelling and control in prostate brachytherapy. *IET Control Theory & Applications*, *6*(*11*), 1671–1681.
Mahvash, M. & Dupont, P. (2009). Fast needle insertion to minimize tissue deformation and damage. In *Proceedings of IEEE international conference on robotics and automation*, pp. 3097–3102.
Mahvash, M., & Dupont, P. (2010). Mechanics of dynamic needle insertion into a biological material. *IEEE Transactions on Biomedical Engineering*, *57*(*4*), 934–943.
Majewicz, A. et al. (2014). Design and evaluation of duty-cycling steering algorithms for robotically-driven steerable needles. In *Proceedings of IEEE international conference on robotics and automation*, pp. 5883–5888.
Mallapragada, V., Sarkar, N., & Podder, T. (2009). Robot-assisted real-time tumor manipulation for breast biopsy. *IEEE Transactions on Robotics*, *25*(*2*), 316–324.
Maurin, B. et al. (2004). In vivo study of forces during needle insertions. In *Proceedings of the medical robotics, navigation and visualisation scientific workshop*, pp. 1–8.
McGill, C. et al. (2012). Effects of insertion speed and trocar stiffness on the accuracy of needle position for brachytherapy. *Medical Physics*, *39*(*4*), 1811–1817.
Meltsner, M. et al. (2007). Observations on rotating needle insertions using a brachytherapy robot. *Physics in Medicine and Biology*, *52*(*19*), 6027.
Minhas, D. et al. (2007). Modeling of needle steering via duty-cycled spinning. In *Proceedings of* annual international conference of the IEEE engineering in medicine and biology society, pp. 2756–2759.
Misra, S. et al. (2008). Modeling of tool-tissue interactions for computer-based surgical simulation: A literature review. *Presence: Teleoperators and Virtual Environments*, *17*(*5*), 463–491.
Misra, S. et al. (2008). Needle-tissue interaction forces for bevel-tip steerable needles. In *Proceedings of* IEEE RAS & EMBS *international conference on biomedical robotics and biomechatronics*, pp. 224–231.
Misra, S. et al. (2010). Mechanics of flexible needles robotically steered through soft tissue. *The International Journal of Robotics Research*, *29*(*13*), 1640–1660.
Moore, J. et al. (2011). Hollow needle tissue insertion force model. *CIRP Annals-Manufacturing Technology*, *60*(*1*), 157–160.
Moreira, P., & Misra, S. (2015). Biomechanics-based curvature estimation for ultrasound-guided flexible needle steering in biological tissues. *Annals of Biomedical Engineering*, *43*(*8*), 1716–1726.
Morgan, J. et al. (2004). Robotic techniques improve quality of life in patients undergoing atrial septal defect repair. *The Annals of Thoracic Surgery*, *77*(*4*), 1328–1333.
Morimoto, M. et al. (2010). C-arm cone beam CT for hepatic tumor ablation under real-time 3D imaging. *American Journal of Roentgenology*, *194*(*5*), W452–W454.
Motaharifar, M. et al. (June 2012). Adaptive observer-based controller design for a class of nonlinear systems with application to image guided control of steerable needles. In *Proceedings of American control conference*, pp. 4849–4854.
Muntener, M. et al. (2006). Magnetic resonance imaging compatible robotic system for fully automated brachytherapy seed placement. *Urology*, *68*(*6*), 1313–1317.
Nag, S. et al. (2004). Proposed guidelines for image-based intracavitary brachytherapy for cervical carcinoma: Report from image-guided brachytherapy working group. *International Journal of Radiation Oncology* Biology* Physics*, *60*(*4*), 1160–1172.
Neshat, H. & Patel, R. (2008). Real-time parametric curved needle segmentation in 3D ultrasound images. In *Proceedings of IEEE RAS & EMBS international conference on biomedical robotics and biomechatronics* , pp. 670–675.
Neubach, Z., & Shoham, M. (2010). Ultrasound-guided robot for flexible needle steering. *IEEE Transactions on Biomedical Engineering*, *57*(*4*), 799–805.
Nguyen, N. et al. (2001). Laparoscopic versus open gastric bypass: A randomized study of outcomes, quality of life, and costs. *Annals of Surgery*, *234*(*3*), 279–291.
Nicolau, S. et al. (2005). A complete augmented reality guidance system for liver punctures: First clinical evaluation. In *Proceedings of international conference on medical image computing and computer-assisted intervention* , pp. 539–547.
Nicolau, S. et al. (2009). An augmented reality system for liver thermal ablation: Design and evaluation on clinical cases. *Medical Image Analysis*, *13*(*3*), 494–506.
Nicolau, S. et al. (2011). Augmented reality in laparoscopic surgical oncology. *Surgical Oncology*, *20*(*3*), 189–201.
Nifong, W. et al. (2003). Robotic mitral valve repair: Experience with the da vinci system. *The Annals of Thoracic Surgery*, *75*(*2*), 438–443.
Nikou, C. et al. (2000). Augmented reality imaging technology for orthopaedic surgery. *Operative Techniques in Orthopaedics*, *10*(*1*), 82–86.
Nisky, I. et al. (2011). Perception and action in teleoperated needle insertion. *IEEE Transactions on Haptics*, *4*, 155–166.
Novotny, P. et al. (2007). GPU based real-time instrument tracking with three-dimensional ultrasound. *Medical Image Analysis*, *11*(*5*), 458–464.
Okamura, A. et al. (2004). Force modeling for needle insertion into soft tissue. *IEEE Transactions on Biomedical Engineering*, *51*(*10*), 1707–1716.
Okazawa, S. et al. (2005). Hand-held steerable needle device. *IEEE/ASME Transactions on Mechatronics*, *10*(*3*), 285–296.
Okazawa, S. et al. (2006). Methods for segmenting curved needles in ultrasound images. *Medical Image Analysis*, *10*(*3*), 330–342.
Park, S. & Lee, S. (2007). Disturbance observer based robust control for industrial robots with flexible joints. In International Conference on Control, Automation and Systems, pp. 584–589.
Park, W. et al. (2005). Diffusion-based motion planning for a nonholonomic flexible needle model. In IEEE International Conference on Robotics and Automation, pp. 4600–4605.
Park, Y. et al. (2008). MRI-compatible haptics: Feasibility of using optical fiber bragg grating strain-sensors to detect deflection of needles in an mri environment. *International Society for Magnetic Resonance in Medicine (ISMRM) 2008*.
Park, W. et al. (2009). The path-of-probability algorithm for steering and feedback control of flexible needles, The International journal of robotics research.
Patil, S. & Alterovitz, R. (2010). Interactive motion planning for steerable needles in 3D environments with obstacles. In *Proceedings of IEEE RAS and EMBS international conference on biomedical robotics and biomechatronics*, pp. 893–899.
Patil, S. et al. (2014). Needle steering in 3D via rapid replanning. *IEEE Transactions on Robotics*, *30*(*4*), 853–864.
Patriciu, A. et al. (2007). Automatic brachytherapy seed placement under mri guidance. *IEEE Transactions on Biomedical Engineering*, *54*, 1499–1506.
Phee, L. et al. (2006). Ultrasound guided robotic biopsy of the prostate. *International Journal of Humanoid Robotics*, *3*(*04*), 463–483.
Piccin, O. et al. (2009). A force feedback teleoperated needle insertion device for percutaneous procedures. *The International Journal of Robotics Research*, *28*(*9*), 1154–1168.
Podder, T. et al. (2005). Effects of velocity modulation during surgical needle insertion. In *Proceedings of conference of the engineering in medicine and biology society* , pp. 1–4.
Podder, T. et al. (2014). AAPM and GEC-ESTRO guidelines for image-guided robotic brachytherapy: Report of task group 192. *Medical Physics*, *41*(*10*), 101501.
Pouliot, J. et al. (2004). Inverse planning for HDR prostate brachytherapy used to boost dominant intraprostatic lesions defined by magnetic resonance spectroscopy imaging. *International Journal of Radiation Oncology* Biology* Physics*, *59*(*4*), 1196–1207.
Qiu, W. et al. (2008). Needle segmentation using 3D quick randomized hough transform. In *Proceedings of international conference on intelligent networks and intelligent systems*, pp. 449–452.
Reed, K. et al. (2008). Integrated planning and image-guided control for planar needle steering. In *Proceedings of the 2nd IEEE RAS & EMBS international conference on biomedical robotics and biomechatronics* , pp. 819–824.
Reed, K. et al. (2009). Controlling a robotically steered needle in the presence of torsional friction. In *Proceedings of* IEEE *international conference on robotics and automation*, pp. 3476–3481, IEEE.
Reed, K. et al. (2009). Modeling and control of needles with torsional friction. *IEEE Transactions on Biomedical Engineering*, *56*(*12*), 2905–2916.
Reed, K. et al. (2011). Robot-assisted needle steering. *IEEE Robotics & Automation Magazine*, *18*(*4*), 35–46.
Roesthuis, R. et al. (2012). Mechanics-based model for predicting in-plane needle deflection with multiple bends. In *Proceedings of the 4th IEEE RAS & EMBS international conference on biomedical robotics and biomechatronics (BioRob)*, pp. 69–74.
Roesthuis, R. et al. (2014). Three-dimensional needle shape reconstruction using an array of fiber bragg grating sensors. *IEEE/ASME Transactions on Mechatronics*, *19*(*4*), 1115–1126.
Rossa, C. et al. (2016). Adaptive quasi-static modelling of needle deflection during steering in soft tissue. *IEEE Robotics and Automation Letters*, *1*, 916–923.
Rossa, C. et al. (2016). Constrained optimal control of needle deflection for semi-manual steering. In *Proceedings of IEEE/ASME international conference onadvanced*

intelligent mechatronics , pp. 1198–1203.
Rossa, C., Lehamnn, T., Sloboda, R., Usmani, N., & Tavakoli, M. (2017). A data-driven soft sensor for needle deflection in heterogeneous tissue using just-in-time modelling. *Medical & Biological Engineering & Computing*. http://dx.doi.org/10.1007/s11517-016-1599-1.
Rossa, C. et al. (2016). Estimating needle tip deflection in biological tissue from a single transverse ultrasound image: Application to brachytherapy. *International Journal of Computer Assisted Radiology and Surgery*, *11*(*07*), 1347–1359.
Rossa, C. et al. (2016). Multiactuator haptic feedback on the wrist for needle steering guidance in brachytherapy. *IEEE Robotics and Automation Letters*, *1*, 852–859.
Rossa, C., Usmani, N., Sloboda, R., & Tavakoli, M. (2017). A hand-held assistant for semi-automated percutaneous needle steering. *IEEE Transactions on Biomedical Engineering*, *64*, 637–648.
Rucker, C. et al. (2011). Deflection-based force sensing for continuum robots: A probabilistic approach. In *Proceedings of* IEEE/RSJ *international conference on intelligent robots and systems*, pp. 3764–3769.
Rucker, C. et al. (2013). Sliding mode control of steerable needles. *IEEE Transactions on Robotics*, *29*(*5*), 1289–1299.
Salcudean, S. et al. (2008). A robotic needle guide for prostate brachytherapy. In *Proceedings of* IEEE *international conference on robotics and automation*, pp. 2975–2981.
Schneider, C. et al. (2004). A robotic system for transrectal needle insertion into the prostate with integrated ultrasound. In *Proceedings of IEEE international conference on robotics and automation*, vol. 1, pp. 365–370.
Seifabadi, R. et al. (2012). Robotic system for MRI-guided prostate biopsy: Feasibility of teleoperated needle insertion and ex vivo phantom study. *International Journal of Computer Assisted Radiology and Surgery*, *7*(*2*), 181–190.
Shah, S. et al. (2008). Robotically assisted needle driver: Evaluation of safety release, force profiles, and needle spin in a swine abdominal model. *International Journal of Computer Assisted Radiology and Surgery*, *3*(*1–2*), 173–179.
Smith, W. et al. (2001). Three-dimensional ultrasound-guided core needle breast biopsy. *Ultrasound in Medicine & Biology*, *27*(*8*), 1025–1034.
Solbiati, L. et al. (1997). Percutaneous US-guided radio-frequency tissue ablation of liver metastases: Treatment and follow-up in 16 patients. *Radiology*, *202*(*1*), 195–203.
Stetten, G., & Chib, V. (2001). Overlaying ultrasonographic images on direct vision. *Journal of Ultrasound in Medicine*, *20*(*3*), 235–240.
Stetten, G. et al. (2001). Real time tomographic reflection: Phantoms for calibration and biopsy. In Augmented Reality. In *Proceedings of IEEE and ACM international symposium on* , pp. 11–19.
Susil, R. et al. (1999). A single image registration method for ct guided interventions. In *Proceedings of international conference on medical image computing and computer-assisted intervention*, pp. 798–808.
Susil, R. et al. (2004). System for prostate brachytherapy and biopsy in a standard 1.5t mri scanner. *Magnetic Resonance in Medicine*, *52*(*3*), 683–687.
Swaney, P. et al. (2013). A flexure-based steerable needle: High curvature with reduced tissue damage. *IEEE Transactions on Biomedical Engineering*, *60*(*4*), 906–909.
Swensen, J. et al. (2014). Torsional dynamics of steerable needles: Modeling and fluoroscopic guidance. *IEEE Transactions on Biomedical Engineering*, *61*(*11*), 2707–2717.
Taylor, R. et al. (2008). Medical robotics and computer-integrated surgery. In *Springer handbook of robotics*, pp. 1199–1222, Springer.
Teber, D. et al. (2009). Augmented reality: A new tool to improve surgical accuracy during laparoscopic partial nephrectomy* Preliminary in vitro vivo results. *European Urology*, *56*(*2*), 332–338.
Tinelli, R. et al. (2011). Robotics versus laparoscopic radical hysterectomy with lymphadenectomy in patients with early cervical cancer: A multicenter study. *Annals of Surgical Oncology*, *18*(*9*), 2622–2628.
Torabi, M. et al. (2009). Guiding medical needles using single-point tissue manipulation. In *Proceedings of* IEEE *international conference on robotics and automation*, pp. 2705–2710.
Turkbey, B. et al. (2009). Imaging localized prostate cancer: Current approaches and new developments. *American Journal of Roentgenology*, *192*(*6*), 1471.
Van de Berg, N. et al. (2015). Design of an actively controlled steerable needle with tendon actuation and fbg-based shape sensing. *Medical Engineering & Physics*, *37*(*6*), 617–622.
Van Sonnenberg, E. et al. (1983). Percutaneous biopsy of difficult mediastinal, hilar, and pulmonary lesions by computed tomographic guidance and a modified coaxial technique. *Radiology*, *148*(*1*), 300–302.
Viswanathan, A. et al. (2012). American brachytherapy society consensus guidelines for locally advanced carcinoma of the cervix. part ii: High-dose-rate brachytherapy. *Brachytherapy*, *11*(*1*), 47–52.
Vitrani, M. et al. (2016). Prostate biopsies assisted by comanipulated probe-holder: First in man. *International Journal of Computer Assisted Radiology and Surgery*, 1–9.
Vrooijink, G. et al. (2014). Needle path planning and steering in a three-dimensional non-static environment using two-dimensional ultrasound images. *The International Journal of Robotics Research* (0278364914526627).
Wacker, F. et al. (2006). An augmented reality system for MR image-guided needle biopsy: Initial results in a swine model 1. *Radiology*, *238*(*2*), 497–504.
Waine, M. et al. (July 2016). An integrator-backstepping control approach for out-of-plane beedle deflection minimization. In *Proceedings of IEEE/ASME international conference onadvanced intelligent mechatronics* , pp. 1598–1603.
Waine, M. et al. (2016). Needle tracking and deflection prediction for robot-assisted needle insertion using 2D ultrasound images. *Journal of Medical Robotics Research*, *1*(*01*), 1640001.
Waine, M. et al. (2016). Needle tracking and deflection prediction for robot-assisted needle insertion using 2D ultrasound images. *Journal of Medical Robotics Research*, *01*(*01*), 1640001.
Waine, M. et al. (2016). Three-dimentional needle shape estimation in trus-guided prostate brachytherapy using 2d ultrasound images. *IEEE Journal of Biomedical and Health Informatics*, *6*, 1621–1631.
Wan, G. et al. (2005). Brachytherapy needle deflection evaluation and correction. *Medical Physics*, *32*(*4*), 902–909.
We, Z. et al. (2004). Robot-assisted 3D-TRUS guided prostate brachytherapy: System integration and validation. *Medical Physics*, *31*(*3*), 539–548.
Webster, R. et al. (2006). Nonholonomic modeling of needle steering. *The International Journal of Robotics Research*, *25*(*5–6*), 509–525.
Wedlick, T. & Okamura, A. (2009). Characterization of pre-curved needles for steering in tissue. In *Proceedings of international conference of the IEEE engineering in medicine and biology society* , pp. 1200–1203.
Wei, Z. et al. (2004). Robotic-aided 3D TRUS guided intraoperative prostate brachytherapy. In *Medical Imaging 2004*, pp. 361–370, International Society for Optics and Photonics.
Weiss, C. et al. (2011). Augmented reality visualization using image-overlay for mr-guided interventions: System description, feasibility, and initial evaluation in a spine phantom. *American Journal of Roentgenology*, *196*(*3*), W305–W307.
West, J., & Maurer, C. (2004). Designing optically tracked instruments for image-guided surgery. *IEEE Transactions on Medical Imaging*, *23*(*5*), 533–545.
Wood, N. et al. (Aug 2010). Needle steering system using duty-cycled rotation for percutaneous kidney access. In *Proceedings of annual international conference of the IEEE engineering in medicine and biology*, pp. 5432–5435.
Xu, K., & Simaan, N. (2008). An investigation of the intrinsic force sensing capabilities of continuum robots. *IEEE Transactions on Robotics*, *24*(*3*), 576–587.
Xu, K., & Simaan, N. (2010). Intrinsic wrench estimation and its performance index for multisegment continuum robots. *IEEE Transactions on Robotics*, *26*, 555–561.
Xu, J. et al. (2008). Motion planning for steerable needles in 3D environments with obstacles using rapidly-exploring random trees and backchaining. In *Proceedings of* IEEE *international conference on automation science and engineering*, pp. 41–46.
Xu, S. et al. (2008). Real-time mri-trus fusion for guidance of targeted prostate biopsies. *Computer Aided Surgery*, *13*(*5*), 255–264.
Xu, J. et al. (2009). Planning fireworks trajectories for steerable medical needles to reduce patient trauma. In *Proceedings of IEEE/RSJ international conference on intelligent robots and systems*, pp. 4517–4522.
Yan, K. et al. (2006). An improved needle steering model with online parameter estimator. *International Journal of Computer Assisted Radiology and Surgery*, *1*(*4*), 205–212.
Yan, K. et al. (2006). Needle steering modeling and analysis using unconstrained modal analysis. In *Proceedings of IEEE/RAS-EMBS international conference on biomedical robotics and biomechatronics*, pp. 87–92.
Yan, K. et al. (2009). Flexible needle-tissue interaction modeling with depth-varying mean parameter: Preliminary study. *IEEE Transactions on Biomedical Engineering*, *56*(*2*), 255–262.
Yu, Y. et al. (2006). Robot-assisted prostate brachytherapy. In *Medical Image Computing and Computer-Assisted Intervention*, pp. 41–49, Springer.
Zarrad, W. et al. (Oct 2007). Towards teleoperated needle insertion with haptic feedback controller. In *Proceedings of IEEE/RSJ international conference on intelligent robots and systems*, pp. 1254–1259.
Zhao, Y. et al. (2012). Tracking micro tool in a dynamic 3D ultrasound situation using kalman filter and ransac algorithm. In *Proceedings of IEEE international symposium on biomedical imaging*, pp. 1076–1079.
Zhou, H. et al. (2008). Automatic needle segmentation in 3D ultrasound images using 3D improved hough transform, in *Medical Imaging*, pp. 691821–691821, International Society for Optics and Photonics.